



Enhanced upward motion through the troposphere over the tropical western Pacific and its implications for the transport of trace gases from the troposphere to the stratosphere

Kai Qie¹, Wuke Wang^{2,3}, Wenshou Tian¹, Rui Huang¹, Mian Xu¹, Tao Wang¹, and Yifeng Peng¹

¹College of Atmospheric Sciences, Lanzhou University, Lanzhou 730000, China

²Department of Atmospheric Science, China University of Geosciences, Wuhan 430074, China

³Centre for Severe Weather and Climate and Hydro-Geological Hazards, 430074 Wuhan, China

Correspondence: Wuke Wang (wangwuke@cug.edu.cn)

Received: 1 August 2021 – Discussion started: 2 September 2021

Revised: 7 March 2022 – Accepted: 9 March 2022 – Published: 5 April 2022

Abstract. The tropical western Pacific (TWP) is a preferential area of air uplifting from the surface to the upper troposphere. A significantly intensified upward motion through the troposphere over the TWP in the boreal wintertime (November to March of the following year, NDJFM) has been detected using multiple reanalysis datasets. The upward motion over the TWP is intensified at rates of 8.0 ± 3.1 % per decade and 3.6 ± 3.3 % per decade in NDJFM at 150 hPa from 1958 to 2017, using JRA55 and ERA5 reanalysis datasets, while the MERRA-2 reanalysis data show a 7.5 ± 7.1 % per decade intensified upward motion for the period 1980–2017. Model simulations using the Whole Atmosphere Community Climate Model, version 4 (WACCM4), suggest that warming global sea surface temperatures (SSTs), particularly SSTs over the eastern maritime continent and tropical western Pacific, play a dominant role in the intensification of the upward motion by strengthening the Pacific Walker circulation and enhancing the deep convection over the TWP. Using CO as a tropospheric tracer, the WACCM4 simulations show that an increase in CO at a rate of 0.4 ppbv (parts per billion by volume) per decade at the layer 150–70 hPa in the tropics is mainly resulted from the global SST warming and the subsequent enhanced upward motion over the TWP in the troposphere and strengthened tropical upwelling of Brewer–Dobson (BD) circulation in the lower stratosphere. This implies that more tropospheric trace gases and aerosols from both natural maritime sources and outflow from polluted air from South Asia may enter the stratosphere through the TWP region and affect the stratospheric chemistry and climate.

1 Introduction

The tropical western Pacific (TWP) is a critical region for tropical and global climate (e.g. Webster et al., 1996; Hu et al., 2020). It has the largest area of warm sea surface temperature (exceeding 28 °C) which fuels intense and massive deep convection and is thus the largest source of latent heat and water vapour into the atmosphere (Webster and Lukas, 1992). The TWP region is also the most important source of tropospheric air entering the stratosphere due to the strong upward motion and deep convection over

this region (e.g. Fueglistaler et al., 2004; Pan et al., 2016). Through the TWP region, tropospheric trace gases, e.g. the natural maritime bromine-containing substances and outflow from anthropogenic emissions from South Asia, are lifted to the upper troposphere and lower stratosphere (UTLS) by the strong upward motion and the deep convection and, subsequently, into the stratosphere by the large-scale upwelling (e.g. Levine et al., 2007, 2008; Navarro et al., 2015), which affects the ozone concentration and other chemical processes in the stratosphere (e.g. Feng et al., 2007; Sinnhuber et al., 2009). At the same time, the TWP region has the lowest cold-

point tropopause temperature (CPTT) over the globe and plays an important role in controlling the water vapour concentration in the stratosphere (e.g. Fueglistaler et al., 2009; Newell and Gould-Steward, 1981; Pan et al., 2016; Randel and Jensen, 2013). The TWP is an important region for tropospheric trace gases being transported from the troposphere to the stratosphere, and therefore influences the stratospheric chemistry (e.g. Fueglistaler et al., 2004; Levine et al., 2007; Krüger et al., 2008; Pan et al., 2016).

The TWP was thought to be the main pathway of the troposphere-to-stratosphere transport. The concept of a stratospheric fountain was proposed by Newell and Gould-Steward (1981), which suggested that the water-vapour-poor air in the stratosphere stems mainly from the TWP region. However, subsequent studies, using the observational and reanalysis data, showed that there is subsidence at the near-tropopause level over the maritime continent, which is named the stratospheric drain (Gettelman et al., 2000; Sherwood, 2000; Fueglistaler et al., 2004). Further studies verified that the large-scale transport from the tropical tropopause layer (TTL) to the stratosphere is dominated by the upward branch of the Brewer–Dobson (BD) circulation (Brewer, 1949; Dobson, 1956; Holton et al., 1995), while the local upwelling may play a minor role (e.g. Levine et al., 2007; Fueglistaler et al., 2009; Schoeberl et al., 2018).

Though the vertical transport from TTL to the lower stratosphere is dominated by the BD circulation, numerous studies confirmed that the TWP region is an important pathway of the surface air entering the TTL (Fueglistaler et al., 2004; Levine et al., 2007; Krüger et al., 2008; Haines and Esler, 2014). Based on a trajectory model, Fueglistaler et al. (2004) pointed out that approximately 80 % of the trajectories ascending into the stratosphere from the TTL are originated from the TWP region. Bergman et al. (2012) suggested that the tropospheric air over the TWP enters the stratosphere mainly in boreal winter, while less air over the TWP could be transported into the stratosphere during boreal summer. Other studies also found that the TWP region is an important source of the tropospheric trace gases in the TTL (e.g. Newton et al., 2018; Pan et al., 2016; Wales et al., 2017), and even the polluted air from East Asia could be transported rapidly to Southeast Asia by meridional winds and, subsequently, be elevated to the tropical upper troposphere by the strong upward motion and the deep convection (Ashfold et al., 2015). Hence, the strength of the upward motion over the TWP region during boreal winter is a key feature for understanding the variations in trace gases in the TTL and is therefore important for stratospheric chemistry and climate.

The strength of the TWP upward motion is closely related to atmospheric circulation and deep convection. The ascending branch of the Pacific Walker circulation and the strong deep convection over the TWP allow rapid transport from the surface to the upper troposphere (Hosking et al., 2012). In association with global warming, atmospheric circulation, deep convection, and the boundary conditions (e.g. sea sur-

face temperature – SST) have been changed. For example, the Hadley cell has been extended to the subtropics, and the Walker circulation over the Pacific has been shifted westward over the past few decades (e.g. Lu et al., 2007; Garfinkel et al., 2015; Ma and Zhou, 2016). At the same time, SSTs over most of areas are becoming warmer (Cane et al., 1997; Deser et al., 2010), which modulates the deep convection and atmospheric wave activities in the troposphere and then leads to changes in atmospheric circulations from the troposphere and the stratosphere (e.g. Garfinkel et al., 2013; Xie et al., 2012, 2014a; Wang et al., 2015; Hu et al., 2016; Lu et al., 2020). However, how the strength of the upward motion in the lower TTL over the TWP region has been changed over the past few decades remains unclear. In this study, we investigate the long-term trend of the upward motion over the TWP using JRA55, ERA5, and MERRA-2 reanalysis datasets and different WACCM4 simulations, as described in Sect. 2. The implication of the changes in the upward motion over the TWP to the transport of trace gases from the surface to the UTLS will be discussed in Sect. 3.

2 Data and method

2.1 Reanalysis data

To investigate the long-term trend of the upward motion over the TWP through the troposphere, three most recent reanalysis datasets, including JRA55, from the Japan Meteorological Agency (JMA), ERA5, from the European Centre for Medium-Range Weather Forecasting (ECMWF), and MERRA-2, from the National Aeronautics and Space Administration/Global Modeling and Assimilation Office (NASA/GMAO), are used in this study (Table 1). The JRA55 data, covering the period from 1958 to the present, are interpolated to the standard pressure levels and $1.25^\circ \times 1.25^\circ$ horizontal mesh (Harada et al., 2016). The ERA5 reanalysis is the newest generation product from the ECMWF (Hersbach et al., 2020). The ERA5 data are based on the Integrated Forecast System (IFS), Cy41r2, which includes the improved model physics, core dynamics, and data assimilation. The ERA5 data also extend back to 1958, which coincides with the time that radiosonde observations in the Arctic became more systematic and regular. It should be noted that the ERA5 data suffer from a bias during 2000–2006 and are replaced by the ERA5.1 data in this period here. The MERRA-2 data are also used (Gelaro et al., 2017), which are produced by NASA/GMAO, using the Goddard Earth Observing System model (GEOS). Although the horizontal and vertical resolution of MERRA-2 data are similar to MERRA data, the MERRA-2 data represent UTLS processes better (Gelaro et al., 2017). The monthly mean air temperature, horizontal wind fields, and vertical velocity at different pressure levels are extracted from the three reanalysis datasets. In the present study, we mainly focus on the upward motion over TWP region in NDJFM (November–March), which is de-

fined as 20° S–10° N, 100° E–180°, due to the strong upward motion (Fig. 1) and significantly increasing trends of the upward motion (Fig. 2) over there.

Special caution is needed because of the limitations of the reanalysis data. The reanalysis datasets assimilate observational data based on the ground- and space-based remote sensing platforms to provide more realistic data products. However, previous studies suggested that there are still uncertainties in the reanalysis data (e.g. Simmons et al., 2014; Long et al., 2017; Uma et al., 2021). The accuracy of the vertical velocity in reanalysis data sets has been evaluated by the Reanalysis Intercomparison Project (Fujiwara et al., 2017), which is initiated by the Stratosphere–troposphere Processes And their Role in Climate (SPARC). Results of a comparison between the radar-observed data and the reanalysis data indicate that the updrafts in the UTLS are captured well near the TWP, even though there are still large biases in the reanalysis datasets, and the updrafts from the JRA55 data are stronger than those from the ERA5 and MERRA-2 data (Uma et al., 2021). Additionally, discontinuities in the reanalysis data due to different observing systems (for example, transition from TOVS, TIROS Operational Vertical Sounder, to Advanced TIROS Operational Vertical Sounder, ATOVS) may still exist (e.g. Long et al., 2017), which could lead to uncertainties in the long-term trend of a certain meteorological field. Hitchcock (2019) suggested that the reanalysis uncertainty is larger in the radiosonde era (after 1958) than in the satellite era (after 1979), but the radiosonde era is of equivalent value to the satellite era because of the dynamical uncertainty dominates in the both eras. The data in the radiosonde era (1958–1978) used in the present study may induce uncertainties in our results. Therefore, we discuss the trends for the periods of both 1958–2017 and 1980–2017. In addition, we combine the three most recent reanalysis datasets (JRA55, ERA5, and MERRA-2) to obtain relatively robust results.

2.2 Observed CO data

Since CO has a photochemical lifetime in the range of 2–3 months (Xiao et al., 2007), it could be utilized as a tracer of cross-region transport in the troposphere and the lower stratosphere (Park et al., 2009). Here, CO is used as a tropospheric tracer to indicate the vertical transport from the near-surface to the upper troposphere and the lower stratosphere. The CO data used in the present study are from space-borne Microwave Limb Sounder (MLS; Livesey et al., 2015) observation and the Measurements of Pollution in the Troposphere instrument (MOPITT; Deeter et al., 2019). MLS is carried by Aura, which has a sun-synchronous orbit at 705 km, with a 16 d repeat cycle. MLS observations are made from 82° S to 82° N and cover the period from 2005 to the present. MLS provides the CO data from the upper troposphere to the mesosphere. The MLS CO v4 level 1 data used in the present study are processed using the recommended procedures (Livesey et al., 2015) and interpolated into a 5° × 5°

horizontal mesh. MOPITT CO data are also used for comparison. The MOPITT instrument is aboard on the Terra satellite, permitting retrievals of CO vertical profiles using both thermal-infrared and near-infrared measurements and has a field of view of 22 km × 22 km. The Terra satellite was launched in 1999, with a 705 km sun-synchronous orbit. MOPITT provides the CO data from the surface to the upper troposphere during the period of 2000/2003 to the present. Here, we use the daytime only MOPITT v8 level 3 CO data. For comparison, we focus on the CO concentrations in MLS and MOPITT data at a similar level (215 hPa in MLS data and 200 hPa in MOPITT data, respectively).

2.3 SST and outgoing longwave radiation (OLR) data

SST data are used in this study to investigate the relationship between the upward motion and SSTs. The SST data are from the Hadley Centre Sea Ice and Sea Surface Temperature data set (HadISST; 1° × 1° horizontal mesh) during 1958–2018 (Rayner et al., 2003). OLR is often utilized to reflect the deep convection in the tropics. The OLR data are extracted from NOAA Interpolated OLR dataset on a 2.5° × 2.5° horizontal mesh during November 1974–March 2018 (Liebmann and Smith, 1996).

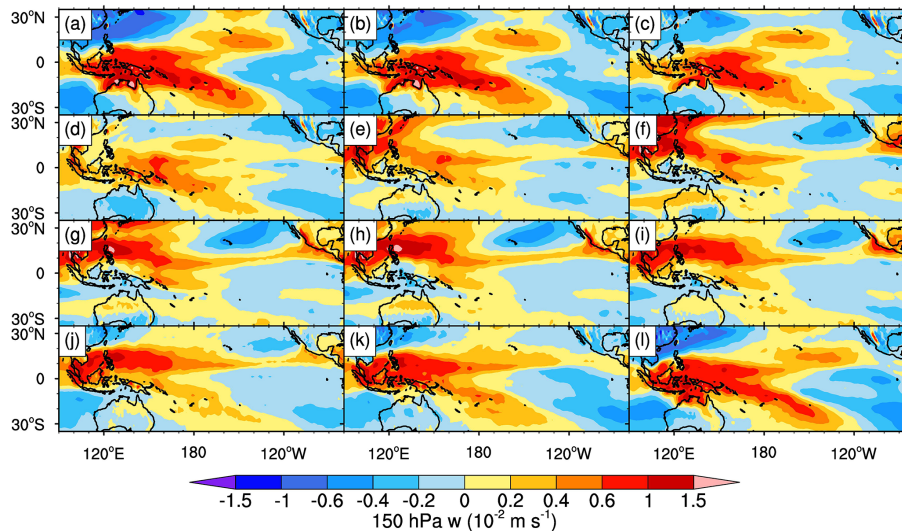
2.4 Model simulations

A series of model simulations with the Whole Atmosphere Community Climate Model version 4 (WACCM4) are performed to find out the main impact factors of the trend of the upward motion over the TWP (Table 2). The WACCM4 is a chemical climate model with a horizontal resolution of 1.9° × 2.5° (Marsh et al., 2013). The WACCM4 has 66 vertical levels from the surface to 145 km, with a vertical resolution of approximately 1 km in the UTLS, which is numerously used to investigate the transport of the trace gases from the troposphere to the stratosphere (e.g. Randel et al., 2010; Xie et al., 2014b; Minganti et al., 2020). A hind-cast simulation (Control simulation) is performed with observed greenhouse gases, solar irradiances, and prescribed SSTs (HadISST dataset is used) during 1955–2018. A single-factor controlling simulation (Fixsst simulation) is done for the same period with the same forcings, except that the global SSTs are fixed to the climatological mean values during 1955–2018 (long-term mean for each calendar month during 1955–2018).

To figure out the impact of the warming SST over the TWP region on the intensification of the upward motion over the TWP region, a couple of time slice simulations (R1 and R2) are also integrated for 33 years. The SSTs over the eastern maritime continent and tropical western Pacific (20° S–20° N, 120–160° E) in the boreal wintertime (November to March of the following year, NDJFM) in R1 are prescribed as the climatological mean SSTs during 1998–2017, while the SSTs over other regions are fixed as the climatological mean

Table 1. Basic specifications of JRA55, ERA5, and MERRA-2 used in this study.

Name	Organization	Time period	Spatial resolution	Temporal resolution	Data assimilation
JRA55	JMA	1958–present	55 km; L60	6 h	4D-Var
ERA5	ECMWF	1950–present	31 km; L137	Hourly	4D-Var
MERRA-2	NASA GMAO	1980–present	$0.5^\circ \times 0.625^\circ$; L72	3 h	3D-Var

**Figure 1.** The climatological mean (averaged over 1958–2017) values of 150 hPa w (10^{-2} m s^{-1}) in January–December (a–l), as derived from the JRA55 data.

SSTs during 1958–2017. The SSTs in R2 are the same as the SSTs in R1, except that the SSTs over the region ($20^\circ \text{ S}–20^\circ \text{ N}$, $120–160^\circ \text{ E}$) in NDJFM are prescribed as the climatological mean SSTs during 1958–1977. Since the SSTs over the eastern maritime continent and tropical western Pacific ($20^\circ \text{ S}–20^\circ \text{ N}$, $120–160^\circ \text{ E}$) show significantly warming trends, the SSTs during 1998–2017 are higher than the SSTs during 1958–1977 (approximately 0.5 K). Hence, the difference between R1 and R2 reflects the impact of the warmed SSTs over the eastern maritime continent and tropical western Pacific ($20^\circ \text{ S}–20^\circ \text{ N}$, $120–160^\circ \text{ E}$) on the atmospheric circulation. The first 3 years of the numeric simulations are not used in the present study to provide a spin-up.

2.5 Transformed Eulerian mean (TEM) calculation

To diagnose the changes in the BD circulation, the meridional and vertical velocities of the BD circulation are calculated by the TEM equations as follows (Andrews and McIntyre, 1976):

$$v^* = \bar{v} - \frac{1}{\rho} \left(\frac{\rho v' \theta'}{\bar{\theta}_z} \right)_z \quad (1)$$

$$w^* = \bar{w} + \frac{1}{a \cos \varphi} \left(\cos \varphi \frac{v' \theta'}{\bar{\theta}_z} \right)_\varphi \quad (2)$$

where v^* and w^* denote the meridional and vertical velocities of the BD circulation, the overbar represents the zonal mean, the prime denotes the deviation from the zonal mean, and θ , a , φ , and ρ indicate the potential temperature, the radius of the Earth, the latitude, and the standard density.

2.6 Linear trends and the significance test

The linear trends are estimated using a simple least squares regression method. The significances of the correlation coefficients, mean differences, and trends are determined via a two-tailed Student's t test. The confidence interval of trend is calculated using the following equation (Shirley et al., 2004):

$$\left(b - t_{1-\frac{\alpha}{2}}(n-2)\sigma, b + t_{1-\frac{\alpha}{2}}(n-2)\sigma \right),$$

where b is the estimated slope, σ denotes the standard error of the slope, and $t_{1-\frac{\alpha}{2}}(n-2)$ represents the value of t distribution with the degree of freedom equal to $n-2$. α is the two-tailed confidence level. σ is calculated as $\sigma = b \sqrt{\frac{1-r^2}{n-2}}$.

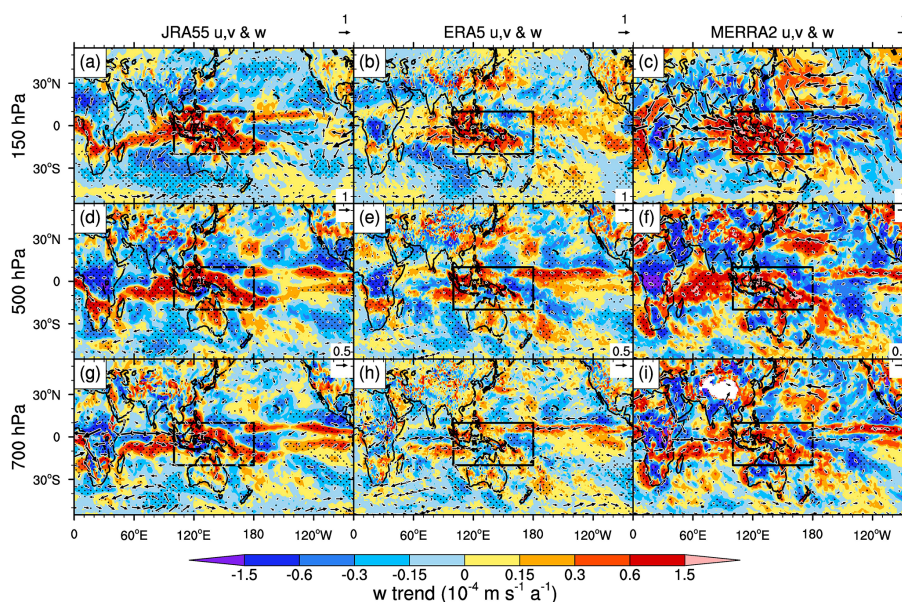


Figure 2. Trends of vertical velocity and horizontal winds at 150, 500, and 700 hPa in NDJFM (November–March), as derived from JRA55, ERA5, and MERRA-2 data. The trends of horizontal winds (arrows; $10^{-1} \text{ m s}^{-1} \text{ a}^{-1}$) and vertical velocity (shading; $10^{-4} \text{ m s}^{-1} \text{ a}^{-1}$) at (a) 150 hPa, (d) 500 hPa, and (g) 700 hPa from JRA55 in NDJFM during 1958–2017 are shown. Panels (b), (e), and (h) are the same as panels (a), (d), and (g) but for the results from ERA5. Panels (c), (f), and (i) are the same as panels (a), (d), and (g), except that the trends are during 1980–2017 and the wind field data are from MERRA-2. The vertical velocity trends over the dotted regions are statistically significant at the 95 % confidence level. The white areas denote missing values. The black rectangles denote the TWP region (20° S – 10° N , 100 – 180° E).

Table 2. Description of simulations with WACCM4.

Experiment	Description
Control	Transient simulation, with observed greenhouse gases and solar irradiances and prescribed SST forcing using observed SST.
Fixsst	Transient simulation, with observed greenhouse gases and solar irradiances and prescribed SST forcing using monthly mean climatology from 1958 to 2017.
R1	Time slice simulation, where SSTs are prescribed as the climatological mean of 1998–2017 over the region (20° S – 20° N , 120 – 160° E) in NDJFM but fixed as the climatological mean for 1958–2017 over other regions.
R2	Same as R1 but the SSTs over the region (20° S – 20° N , 120 – 160° E) are prescribed as the climatological mean SSTs during 1958–1977.

3 Results

3.1 Enhanced upward motion over the TWP

According to previous studies, the lapse rate tropopause is a good proxy for separating the tropospheric and the stratospheric dynamic behaviour (vertical motion dominated and horizontal mixing dominated, respectively) over the TWP (Pan et al., 2019). Since the lapse rate tropopause over the TWP in the boreal winter is near 100 hPa (not shown), we utilize the vertical velocity at 150 hPa to reflect the vertical transport in the upper troposphere. Figure 1 shows the mean

values of the vertical velocity at 150 hPa for each month averaged over 60 years from 1958 to 2017. The TWP region at the UTLS level has a strong upward motion due to the frequent intense deep convection and the Pacific Walker circulation. It is noteworthy that there is strong upward motion at 150 hPa in NDJFM over the TWP, while the upward motion in other months shifts northward, corresponding to the Asia summer monsoon. This is consistent with previous studies (Newell and Gould-Steward, 1981; Bergman et al., 2012). Therefore, we mainly focus on the changes in the upward motion in NDJFM, which is more important to the transport

of air over the TWP from the lower troposphere to the TTL compared to the summer months (as shown in Fig. 1) and, subsequently, to the lower stratosphere. As seen in Fig. 1a–c and k–l, the upward motion (w) at 150 hPa is most evident over the region 20°S – 10°N , 100°E – 180° , which is used to indicate the TWP in the following analysis. The climatological mean 150 hPa vertical velocity (w) in NDJFM in ERA5, during 1958–2017, and MERRA-2, during 1980–2017, are also given in the Supplement (Fig. S1). Comparing with the 150 hPa w in NDJFM using JRA55, the 150 hPa w in ERA5 and MERRA-2 data shows larger values (maximum larger than 1.5 cm s^{-1}) over the land areas but smaller values (minimum less than -0.4 cm s^{-1}) over the marine area. Notably, the 150 hPa w shows no subsidence over the maritime continent, while there is descending motion over the maritime continent at 100 hPa (Fig. S2), which is referred to the stratospheric drain (Gettelman et al., 2000; Sherwood, 2000).

Figure 2 displays the linear trends of w in the upper (150 hPa), middle (500 hPa), and lower (700 hPa) troposphere in NDJFM from 1958 to 2017 using JRA55, ERA5, and MERRA-2 reanalysis datasets. The 150 hPa w increased significantly over most areas of the TWP during 1958–2017 (Fig. 2). At the same time, the upward motion over the TWP in the lower and middle troposphere also mainly shows positive trends (Fig. 2d and g). This indicates that the upward motion over the TWP is increasing through the troposphere from 1958 to 2017. Such an enhancement of the upward motion over the TWP is evident in all three reanalysis datasets used here (JRA55, ERA5, and MERRA-2), although there are also some differences between the three reanalysis datasets. For example, the trends of the horizontal winds in the upper troposphere in MERRA-2 (Fig. 2c) are larger than those in JRA55 and ERA5 (Fig. 2a and b). There are negative trends of vertical velocity in JRA55 and ERA5, while there are positive trends of vertical velocity in MERRA-2 over the northern Pacific. However, these differences are mainly due to the different time periods which are used to calculate the linear trends in JRA55 (1958–2017), ERA5 (1958–2017) and MERRA-2 (1980–2017). Figure S3 gives the trends of w and horizontal winds in NDJFM during 1980–2017 derived from JRA55, ERA5, and MERRA-2 data, which shows insignificant differences between these reanalysis datasets. The trend patterns of the horizontal winds in JRA55, ERA5, and MERRA-2 are consistent with each other (Fig. S3). For the trends of vertical velocity, significantly positive trends over the TWP region can be noted in the JRA55, ERA5, and MERRA-2 datasets, although the trends in ERA5 are slightly weaker than those in JRA55 and MERRA-2 (Figs. 2 and S3). Comparing to the negative trends of the vertical velocity over the central Pacific in JRA55 and ERA5, the negative trends in MERRA-2 extend more northward (Fig. S3).

The time series of the upward motion intensity over the TWP from different datasets are given in Fig. 3. The intensity of the upward motion over the TWP used in Fig. 3 is simply defined as the area-averaged upward mass flux at a specific

level, and the standardized intensity is calculated as the intensity divided by the standard deviation of the intensity at the corresponding level. The intensity of the upward motion over the TWP at 150 hPa increased significantly in NDJFM during last decades, which can be confirmed by all the three reanalysis datasets (Fig. 3). The intensity of the upward motion over the TWP at 150 hPa increased by $3.0 \pm 1.2 \times 10^9\text{ kg s}^{-1}$ per decade ($8.0 \pm 3.1\%$ per decade), $1.3 \pm 1.2 \times 10^9\text{ kg s}^{-1}$ per decade ($3.6 \pm 3.3\%$ per decade), and $3.0 \pm 2.8 \times 10^9\text{ kg s}^{-1}$ per decade ($7.5 \pm 7.1\%$ per decade) in JRA55, ERA5, and MERRA-2 data, respectively (Table 3). As shown in Fig. 3b and c, the intensity of the upward motion at 500 and 700 hPa in JRA55 and the intensity of the upward motion at 500 hPa in ERA5 over the TWP also increased significantly at 95 % confidence level ($4.6 \pm 2.6 \times 10^9$, $2.9 \pm 1.7 \times 10^9$, and $2.5 \pm 2.5 \times 10^9\text{ kg s}^{-1}$ per decade, respectively). The increasing trends in the intensity of the upward motion at 700 hPa in ERA5 and at 500 and 700 hPa in MERRA-2 are significant at the 90 % confidence level at rates of $1.9 \pm 1.6 \times 10^9$, $5.4 \pm 5.3 \times 10^9$, and $3.9 \pm 3.8 \times 10^9\text{ kg s}^{-1}$ per decade, respectively. This suggests a comprehensive enhancement of the vertical velocity through the whole troposphere, which is evident from the surface to 100 hPa (Fig. S4). It can also be inferred that the upward motions over the TWP increased at different rates during the past decades due to the difference between JRA55, ERA5, and MERRA-2 data. Hence, caution is suggested when investigating the trend of the upward motion over the TWP when using the reanalysis data. While the trace gases in the TTL are modulated by the upward motion and subsequent vertical transport (e.g. Garfinkel et al., 2013; Xie et al., 2014b), such a strengthening of the upward motion over the TWP may lead to more tropospheric trace gases in the TTL.

The changes in the atmospheric circulation at the UTLS level in the tropics are closely related to the changes in the tropical deep convection and SSTs (e.g. Levine et al., 2008; Garfinkel et al., 2013; Xie et al., 2020). Here, the trends of the observed OLR provided by NOAA (see Sect. 2) in NDJFM during 1974–2017 are shown in Fig. 4a. Though the time period of the observed OLR data is shorter than the time period we analysed, the changes in OLR could partly reflect the changes in the deep convection during 1958–2017. The OLR shows significantly negative trends over the TWP which indicates intensified deep convection over the TWP. The OLR trend pattern is very similar to the trend pattern of the 150 hPa w (Fig. 2a–c), which indicates that the increasing trends of 150 hPa w are closely related to the intensified deep convection over the TWP. The intensified deep convection not only leads to the strengthened upward motion in the UTLS (Highwood and Hoskins, 1998; Ryu and Lee, 2010) but also results in the decreased temperature near the tropopause, which plays a dominant role in modulating the lower stratospheric water vapour concentration (e.g. Hu et al., 2016; Wang et al., 2016). Corresponding to the enhanced deep convection over the TWP, the CPTT derived

Table 3. The trends of the upward motion over the TWP at 150, 500, and 700 hPa in NDJFM during 1958–2017 from JRA55, ERA5, MERRA-2, the Control simulation, and the Fixsst simulation and the trends of 150 hPa CO from the Control and Fixsst simulations. Note: ppbv – parts per billion by volume.

	JRA55	ERA5	MERRA-2	Control	Fixsst
150 hPa upward motion	$3.0 \pm 1.2 \times 10^9 \text{ kg s}^{-1}$ per decade	$1.3 \pm 1.2 \times 10^9 \text{ kg s}^{-1}$ per decade	$3.0 \pm 2.8 \times 10^9 \text{ kg s}^{-1}$ per decade	$2.0 \pm 1.2 \times 10^9 \text{ kg s}^{-1}$ per decade	$-4.8 \pm 6.4 \times 10^8 \text{ kg s}^{-1}$ per decade
500 hPa upward motion	$4.6 \pm 2.6 \times 10^9 \text{ kg s}^{-1}$ per decade	$2.5 \pm 2.5 \times 10^9 \text{ kg s}^{-1}$ per decade	$5.4 \pm 5.3 \times 10^9 \text{ kg s}^{-1}$ per decade	$3.5 \pm 2.4 \times 10^9 \text{ kg s}^{-1}$ per decade	$-1.0 \pm 1.3 \times 10^9 \text{ kg s}^{-1}$ per decade
700 hPa upward motion	$2.9 \pm 1.7 \times 10^9 \text{ kg s}^{-1}$ per decade	$1.9 \pm 1.6 \times 10^9 \text{ kg s}^{-1}$ per decade	$3.9 \pm 3.8 \times 10^9 \text{ kg s}^{-1}$ per decade	$1.8 \pm 1.4 \times 10^9 \text{ kg s}^{-1}$ per decade	$-6.3 \pm 8.1 \times 10^8 \text{ kg s}^{-1}$ per decade
150 hPa CO	–	–	–	3.4 ppbv per decade	3.2 ppbv per decade

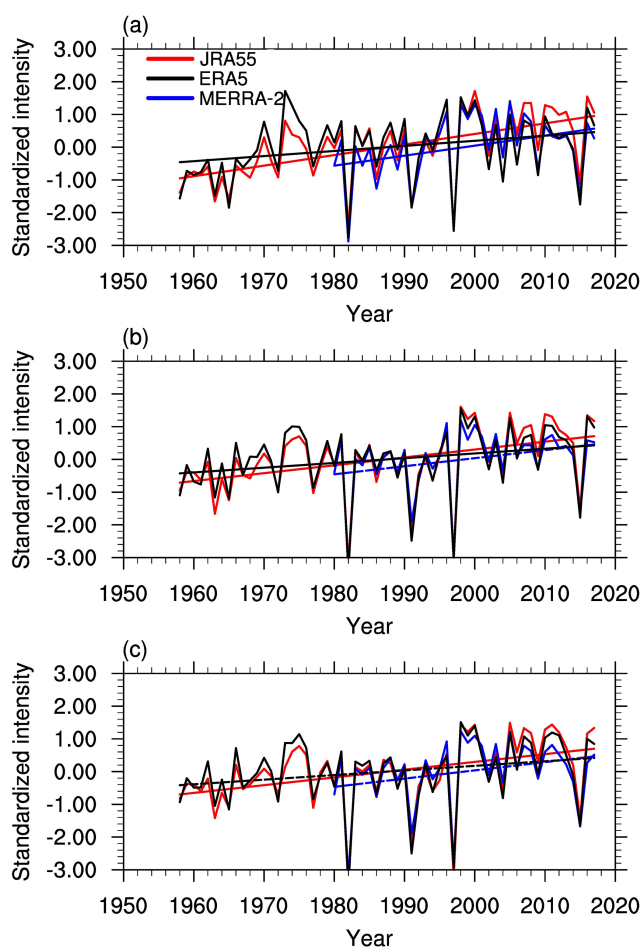


Figure 3. The time series of the standardized intensity of the upward motion over the tropical western Pacific ($20^{\circ} \text{ S} - 10^{\circ} \text{ N}$, $100 - 180^{\circ} \text{ E}$) at (a) 150 hPa, (b) 500 hPa, and (c) 700 hPa extracted from JRA55 (red), ERA5 (black), and MERRA-2 (blue) datasets. The straight lines in each figure indicate the linear trends. The solid lines denote the linear trends that are significant at the 95 % confidence level, while the dashed lines denote the linear trends that are significant at the 90 % confidence level.

from JRA55 data (see Fig. 4b) shows significantly decreasing trends over the TWP in NDJFM during 1958–2017, which is consistent with Xie et al. (2014a). However, negative trends are also found in other regions in low and mid-latitudes, except over the central and eastern Pacific. It should be noted that the CPTT from different reanalysis datasets may show different trends even for the satellite period (Tegtmeier et al., 2020). Additionally, the JRA55 data before 1978 may also lead to uncertainties in the CPTT trends. Caution is needed when discussing the trends of CPTT from reanalysis datasets.

The changes in the deep convection over the tropical Pacific may be related to the changes in the Pacific Walker circulation. The Pacific Walker circulation shows a significant intensification over the past decades (e.g. Meng et al., 2012; L’Heureux et al., 2013; McGregor et al., 2014). The vertical velocity at 500 and 150 hPa shows significantly positive trends over the TWP in NDJFM during 1958–2017 (Fig. 2). Meanwhile, the lower tropospheric zonal wind shows easterly trends over the tropical Pacific, while the upper tropospheric zonal wind shows westerly trends over the tropical Pacific, which suggests a strengthened Pacific Walker circulation and is consistent with previous studies (Hu et al., 2016; Ma and Zhou, 2016).

The strengthened Pacific Walker circulation is closely related to the changes in the SSTs (e.g. Meng et al., 2012; Ma and Zhou, 2016). The trends of the SSTs in NDJFM during 1958–2017 are shown in Fig. 4c. The SST shows significantly warming trends over almost all of the world, except for the central Pacific in NDJFM during 1958–2017. In addition, the intensity of the upward motion over the TWP is significantly correlated with the SST (Fig. 4d), which suggests that the SST has important effects on the upward motion over the TWP. The correlation coefficient in Fig. 4d shows a La-Niña-like pattern and indicates that the El Niño–Southern Oscillation (ENSO) events exert important impacts on the upward motion over the TWP (Levine et al., 2008). The SSTs over the TWP are mainly positively correlated with the upward motion intensity over the TWP, with negative correlations shown over the western maritime continent, while the SSTs over tropical central, eastern Pacific, and Indian Ocean show

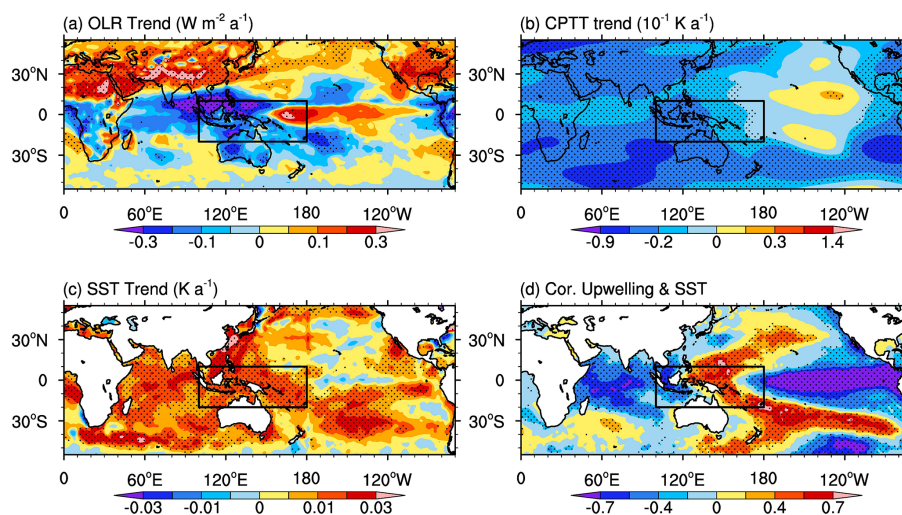


Figure 4. Trends of (a) observed outgoing longwave radiation (OLR; $\text{W m}^{-2} \text{a}^{-1}$) provided by NOAA during 1974–2017. (b) Cold-point tropopause temperature (CPTT; 10^{-1}K a^{-1}) derived from JRA55 data and (c) SST (K a^{-1}) derived from HadISST during 1958–2017 in NDJFM. (d) The correlation coefficients between the intensity of the upward motion at 150 hPa over the TWP and SST in NDJFM during 1958–2017 are shown with the linear trends removed. The trends and correlation coefficients over the dotted regions are statistically significant at the 95 % confidence level. The black rectangles denote the TWP region ($20^{\circ} \text{S}–10^{\circ} \text{N}$, $100–180^{\circ} \text{E}$).

negative correlations with the intensity of the upward motion over the TWP. The SSTs over the Atlantic Ocean are poorly correlated with the upward motion intensity over the TWP (not shown). This result suggests that the changes in global SSTs may be the primary driver of the strengthened Pacific Walker circulation, which leads to enhanced deep convection and intensified upward motion over the TWP.

It could be found that there are extreme minima (1982, 1991, and 1997) in Fig. 3, which may be related to the El Niño events that occurred in these years. To further figure out the impact of ENSO events on the upward motion over the TWP, Fig. S5 displays the time series of the standardized intensity of the upward motion over the TWP at 150, 500, and 700 hPa in NDJFM in JRA55, ERA5, and MERRA-2, with the ENSO signal removed using the linear regression method (Hu et al., 2018; Qie et al., 2021). The extreme minima (1982, 1991, and 1997) become much weaker in Fig. S5 than those in Fig. 3, which indicates that the El Niño events are responsible for the extreme minima. The upward motions over the TWP at 150, 500, and 700 hPa in NDJFM in JRA55, ERA5, and MERRA-2 still show statistically significant increasing trends after removing the ENSO signal in Fig. S5, which suggests that ENSO events exert limited impacts on the trends of the upward motion over the TWP in NDJFM during 1958–2017.

3.2 Simulated trend of the upward motion over the TWP and its potential mechanism

To verify the impact of SST on the trend of the upward motion over the TWP, a couple of model simulations with WACCM4 are employed in the following analysis. Consis-

tent with the results shown using the reanalysis data (Fig. 2a–c), the simulated 150 hPa w (Control simulation) shows significantly increasing trends over the TWP and decreasing trends over the tropical eastern Pacific in NDJFM during 1958–2017 (Fig. 5a). Additionally, the 150 hPa w simulated in the Fixsst simulation shows weak trends over the TWP (Fig. 5b). The difference between the Control and the Fixsst simulations suggests that the trends of the 150 hPa w over the TWP region is dominated by the changes in the global SSTs during 1958–2017. There are also significantly positive trends of the vertical velocity over the TWP in the lower (700 hPa) and middle troposphere (500 hPa) in the Control simulation, while the zonal winds are also enhanced over the tropical Pacific. The vertical velocity over the TWP in the Fixsst simulation shows weak negative trends, and the changes in zonal winds over the tropical Pacific are very weak. This confirms the dominant role of the changes in global SSTs on the enhancement of the Walker circulation.

Previous studies found that the changes in the intensity of the Pacific Walker circulation and the stratospheric residual circulation are closely related to the changes in tropical SST (Meng et al., 2012; Tokinaga et al., 2012; Lin et al., 2015). As suggested by the correlation coefficients between the upward motion at 150 hPa over the TWP and SSTs in Fig. 4d, warmer SSTs over the tropical central and eastern Pacific and Indian Ocean may lead to a weakened upward motion over the TWP (negative correlation). The warming trends of SSTs over the eastern maritime continent and tropical western Pacific may result in an intensification of the upward motion over the TWP. To verify the impact of the changes in the SSTs over eastern maritime continent and tropical western Pacific on

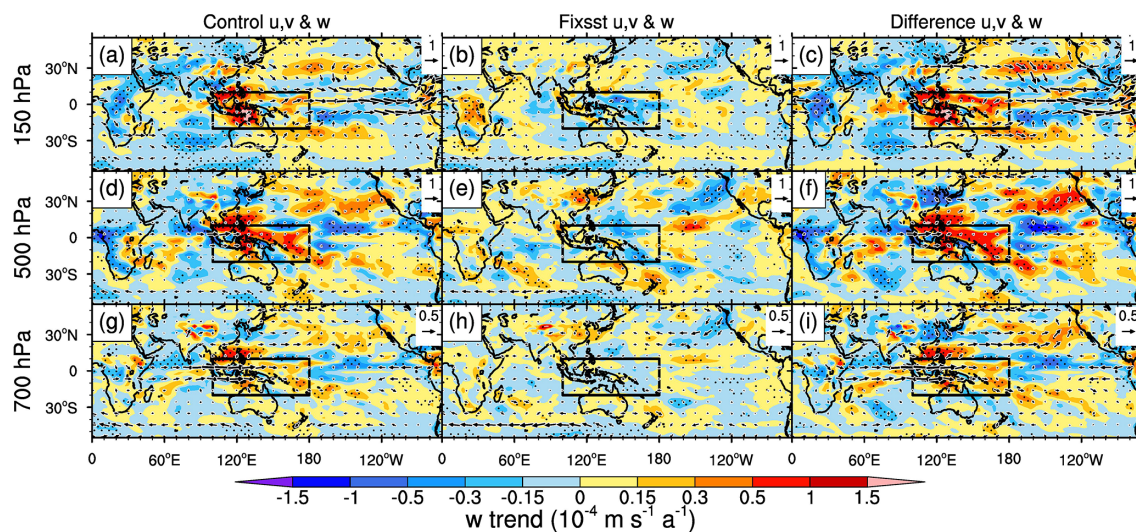


Figure 5. Same as Fig. 2 but for the Control simulation (a, d, and g), Fixsst simulation (b, e, and h), and the difference between the simulations (c, f, and i). The vertical velocity trends over the dotted regions are statistically significant at the 95% confidence level. The black rectangles denote the TWP region (20° S–10° N, 100–180° E).

the trends of the upward motion over the TWP, a couple of single-factor controlling time slice simulations (R1 and R2) performed with only SSTs over the eastern maritime continent and tropical western Pacific (20° S–20° N, 120–160° E) in NDJFM changed in these two simulations. In R1, the SSTs over the eastern maritime continent and tropical western Pacific are prescribed as the climatological mean SSTs during 1958–2017, while the SSTs over the eastern maritime continent and tropical western Pacific in R2 are prescribed as the climatological mean SSTs during 1958–1977 (more details are given in the Sect. 2). The differences in the wind fields between R1 and R2 are shown in Fig. 6. The 150 hPa w shows significantly positive anomalies over the TWP and negative anomalies over the tropical eastern Pacific, which is consistent with the trends of the 150 hPa w in the Control simulation and the reanalysis datasets (Figs. 2 and 5). The upward mass flux over the TWP at 150 hPa increased approximately 27% in the R1, compared with R2, due to the warming SSTs over the eastern maritime continent and tropical western Pacific (approximately 0.5 K). The upward motion in the lower and middle troposphere over the TWP shows increasing trends due to the enhanced convergence induced by the warmer SSTs over the TWP. This result is consistent with Hu et al. (2016), who suggested that the increased zonal gradient of the SSTs over the tropical Pacific could lead to a strengthened Pacific Walker circulation and an enhanced upward motion over the TWP. Therefore, the warmer SSTs over the TWP could contribute largely to the trend of the upward motion over the TWP in NDJFM during 1958–2017.

The changes in the OLR simulated in WACCM4 associated with the changes in the global SSTs are shown in Fig. 7. There is significantly enhanced deep convection, as indicated by OLR over the TWP due to the strengthened convergence

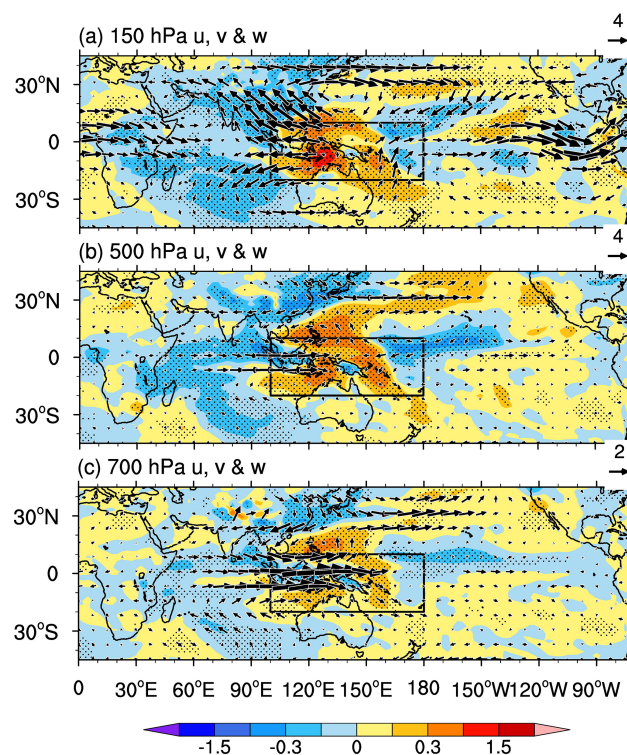


Figure 6. The difference in vertical velocity (shading; 10^{-2} m s^{-1}) and horizontal winds (arrows; m s^{-1}) at (a) 150 hPa, (b) 500 hPa, and (c) 700 hPa in NDJFM between experiments R1 and R2. The differences between the vertical velocity over the dotted regions are statistically significant at the 95% confidence level. The black rectangles denote the TWP region (20° S–10° N, 100–180° E).

in the Control simulation, while the deep convection shows weak and even decreasing trends over the TWP in the Fixsst simulation (Fig. 7a and b). The enhanced deep convection over the TWP could lead to the enhancing trends of the upward motion. Hence, it can be inferred that the changes in the global SSTs are responsible for the intensification of the Pacific Walker circulation and the enhanced deep convection and a stronger upward motion over the TWP, which could extend to the upper troposphere.

3.3 Implications for the concentrations of water vapour and CO in the TTL and lower stratosphere

Previous studies showed that the enhanced deep convection and upward motion could lead to increased CO in the UTLS (e.g. Duncan et al., 2007; Livesey et al., 2013). At the same time, water vapour mixing ratios in the UTLS may increase due to the enhanced upward motion, which could bring more wet air from the low altitude to the high altitude (e.g. Rosenlof, 2003; Lu et al., 2020). However, the water vapour mixing ratios in the lower stratosphere also depend on the tropopause temperature (e.g. Highwood and Hoskins, 1998; Garfinkel et al., 2018; Pan et al., 2019). Hence, the relationship between the intensity of upward motion and the water vapour concentration in the UTLS is complex. Here, the relationship between the trends of the upward motion over the TWP and the changes in CO and water vapour in the UTLS simulated with WACCM4 are analysed.

The trends of CPTT, the 100 hPa stream function, and the water vapour concentration are shown based on the Control and the Fixsst simulation, as well as their difference, in Fig. 7d–i. The changes in the deep convection could lead to the changes in the atmospheric circulation by releasing the latent heat. The changes in the tropical deep convection lead to a Rossby–Kelvin wave response at the UTLS level and then induce the changes in the air temperature near the tropopause (e.g. Gill, 1980; Highwood and Hoskins, 1998). The trends of the 100 hPa stream function show a Rossby wave response over the TWP and a Kelvin wave response over the tropical eastern Pacific in the Control simulation (Fig. 7d), which is caused by the changes in the deep convection over the tropical Pacific. The Rossby–Kelvin wave response further leads to the decrease in the CPTT over the TWP and the increase in the CPTT over the tropical eastern Pacific. Previous studies suggest that the lower stratospheric water vapour is mainly influenced by the coldest temperature near the tropopause (e.g. Garfinkel et al., 2018; Zhou et al., 2021). Since the TWP has the coldest CPTT in the boreal winter (e.g. Pan et al., 2016), the significantly decreased CPTT over the TWP may result in significantly dried lower stratosphere (Fig. 7g). The intensity of the upward motion over the TWP shows negative correlations with the concentration of the tropical lower stratospheric water vapour (not shown). Hence, the enhanced upward motion over the TWP may correspond to a dried lower stratosphere. The CPTT

shows weak trends over the TWP, and the tropical water vapour shows insignificant trends at 70 hPa in the Fixsst simulation. The comparison between the Control simulation and the Fixsst simulation suggests that the trends of the deep convection, the CPTT, and the lower stratospheric water vapour concentration in the tropics in NDJFM during 1958–2017 are dominated by the trends of the global SSTs, while other external forcings may play minor roles.

Generally, the intensified upward motion may lead to more tropospheric trace gases lifting to the upper troposphere and entering the lower stratosphere (e.g. Rosenlof, 2003; Lu et al., 2020). Here we use CO as a tropospheric tracer to detect the possible influences of the enhanced upward motion over the TWP on the transportation of the tropospheric trace gases to the upper troposphere and the lower stratosphere. Due to the data limitations, it is not possible to show the corresponding changes in trace gases by observations in NDJFM during 1958–2017. Here, the trends of CO at around 200 hPa from MOPITT and MLS observations are shown in Fig. 8. The CO increased significantly over the TWP in NDJFM in the upper troposphere from the MOPITT (at 200 hPa during 2000–2017) and MLS data (at 215 hPa during 2005–2017). The concentration of MLS CO over the TWP is approximately 80 ppbv at 215 hPa from MLS observations and 70 ppbv at 200 hPa from MOPITT observations, which is consistent with previous study (e.g. Huang et al., 2016). The MLS CO data show that the area-averaged CO increased by approximately 2.0 ± 3.7 ppbv per decade over the TWP in NDJFM during 2005–2017. The area-averaged MOPITT CO data show a stronger increase by approximately 5.0 ± 3.1 ppbv per decade at 200 hPa from 2000 to 2017 (significant at the 95 % confidence level). It should be pointed out that the linear trends of CO are calculated based on the satellite data which only cover 14 or 18 years due to the data limitations. Hence, the linear trends of CO may have uncertainties, particularly in the regions with large interannual variations. To partially overcome this shortage, the trends of MLS CO at 215 hPa during time periods of 2005–2016, 2006–2016, 2006–2017, and 2007–2016 and the trends of MOPITT CO at 200 hPa during time periods of 2000–2016, 2001–2016, 2001–2017, and 2002–2016 are shown in Fig. S6. It could be found that the CO in the upper troposphere increased robustly over the TWP from both the MLS and MOPITT data. Overall, though the observed CO only covers less than 20 years, the results from the satellite data suggest a possible impact of the intensified upward motion over the TWP on the trace gases in the upper troposphere.

To further illustrate the impacts of the enhanced upward motion on the trace gas in the upper troposphere and lower stratosphere, the Control and Fixsst simulations are used with WACCM4. The trends of the CO concentrations from the Control and Fixsst simulations, as well as their differences, are shown in Fig. 9. The tropical CO at 150 hPa shows significantly increasing trends both in the Control and the Fixsst simulations at rates of 3.4 and 3.2 ppbv per decade, respec-

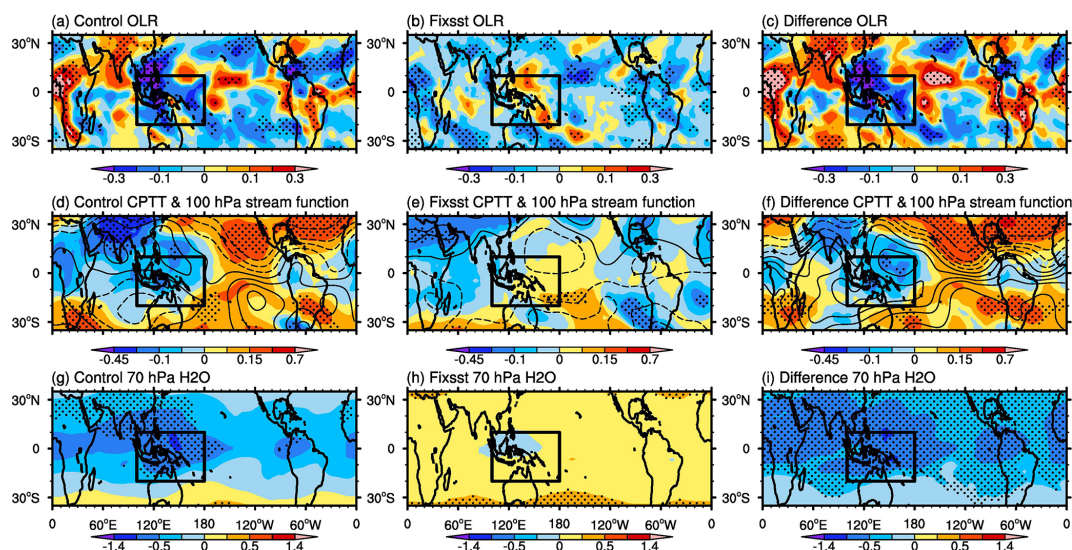


Figure 7. Same as Fig. 5 but for the trends of (a–c) OLR ($\text{W m}^{-2} \text{a}^{-1}$), (d–f) CPTT (shading; 10^{-1}K a^{-1}) and 100 hPa stream function (contour; $10^6 \text{m}^2 \text{s}^{-1} \text{a}^{-1}$), and (g–i) 70 hPa water vapour concentration ($10^{-2} \text{ppmv a}^{-1}$, where ppmv is parts per million by volume). The trends in panels (a)–(c) and (g)–(i) over the dotted regions are statistically significant at the 95 % confidence level. The CPTT trends in panels (d)–(f) over the dotted regions are statistically significant at the 95 % confidence level. The black rectangles denote the TWP region (20°S – 10°N , 100 – 180°E).

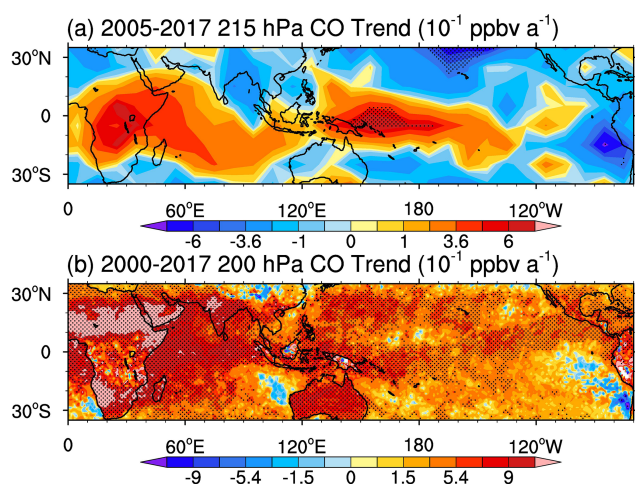


Figure 8. The trends of CO derived from the MOPITT and MLS data. (a) The trends of CO ($10^{-1} \text{ppbv a}^{-1}$) at 215 hPa, using MLS data in NDJFM during 2005–2017. (b) The trends of CO ($10^{-1} \text{ppbv a}^{-1}$) at 200 hPa, using MOPITT data in NDJFM during 2000–2017. The trends of CO over the dotted region are statistically significant at the 90 % confidence level.

tively (Fig. 9a and b). This suggests that the surface emission of the CO exerts the most important effect on the increase in the tropical CO concentration. The differences in the CO trends at 150 hPa between the Control simulation and the Fixsst simulation are also displayed in Fig. 9c. Since the surface emission inventories of the two simulations are the same, it can be inferred that the trends of the CO concen-

tration in Fig. 9c are mainly caused by the changes in the atmospheric circulation induced by the changes in the global SSTs. The difference in the CO concentration at 150 hPa between the Control simulation and the Fixsst simulation shows a significantly increasing trend at a rate of $0.2 \pm 0.1 \text{ppbv}$ per decade over the TWP (significant at the 95 % confidence level). At the same time, decreasing trends over central Africa exist, which resemble the trend patterns of the vertical velocity in the lower TTL and the deep convection (Figs. 5i and 7c). This indicates that the enhanced deep convection in the TWP lead to the strengthened upward motion over the TWP, which results in an extra 6 % in the increasing trend of CO in the upper troposphere over the TWP. It could also be found that CO also increased in the mid-latitudes of the Southern Hemisphere (Fig. 9c). According to previous studies, the CO perturbation from the Indonesian fires at upper troposphere could be transported to the tropical Indian Ocean by easterly winds and then to the subtropics in the Southern Hemisphere through the southward flow during boreal winter. The CO perturbation then spreads rapidly circling the globe following the subtropical jet (Duncan et al., 2007). This is consistent with our results, which show intensified northerlies over the subtropical Indian Ocean (15 – 25°S , 60 – 100°E) at a rate of approximately 0.2m s^{-1} per decade and strengthened westerlies over the subtropical Indian Ocean and western Pacific (20 – 35°N , 60 – 160°E) at a rate of approximately 0.3m s^{-1} per decade (Fig. 5c and f).

The trends of the zonal mean CO concentration from model simulations are displayed in Fig. 10a–c. The zonal mean CO shows significantly increasing trends at all levels

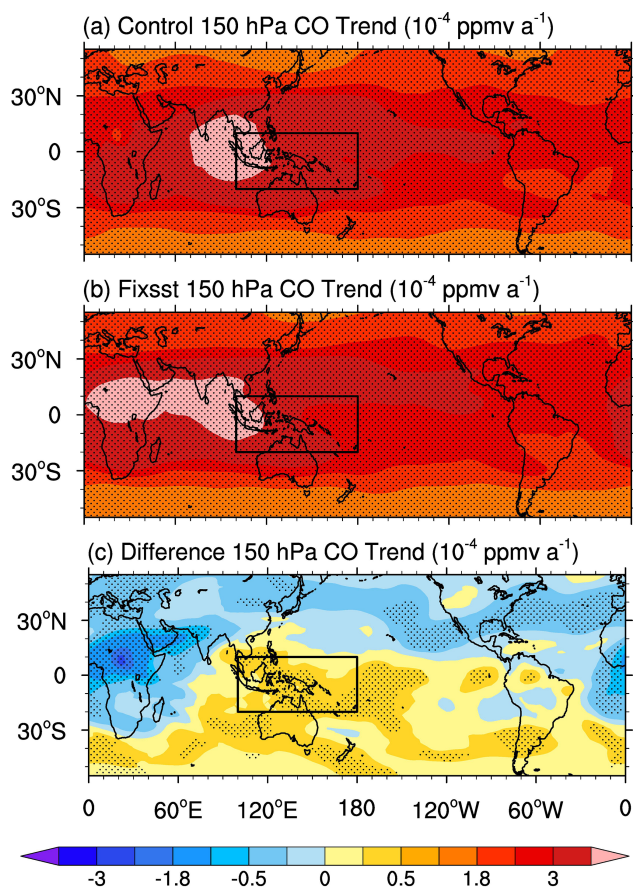


Figure 9. The trends of 150 hPa CO concentration (10^{-4} ppmv a^{-1}) from the (a) Control simulation, (b) Fixsst simulation, and (c) difference between the Control simulation and the Fixsst simulation in NDJFM during 1958–2017. The trends in panels (a)–(c) over the dotted regions are statistically significant at the 95 % confidence level. The black rectangles denote the TWP region (20° S– 10° N, 100 – 180° E).

in the Control simulation and the Fixsst simulation, while the difference in the zonal mean CO between the Control simulation and the Fixsst simulation shows significantly increasing trends in the TTL but negative trends in the middle troposphere in the tropics and the Northern Hemisphere. At the same time, the difference in CO concentration between the Control simulation and the Fixsst simulation averaged in the western Pacific (100 – 180° E) shows significantly increasing trends in the tropics (20° S– 10° N) from the surface to the TTL (Fig. 10f). The CO in the layer 150–70 hPa over the TWP increased by 3.2 and 2.8 ppbv per decade in the Control and Fixsst simulations in NDJFM during 1958–2017, respectively. And the CO difference between the Control and Fixsst simulations increased by 0.4 ± 0.2 ppbv per decade (significant at the 95 % confidence level) in the layer 150–70 hPa over the TWP, which suggests that the intensifying upward motion over the TWP and the tropical upwelling of Brewer–Dobson circulation (BDC) could lead to an increasing trend

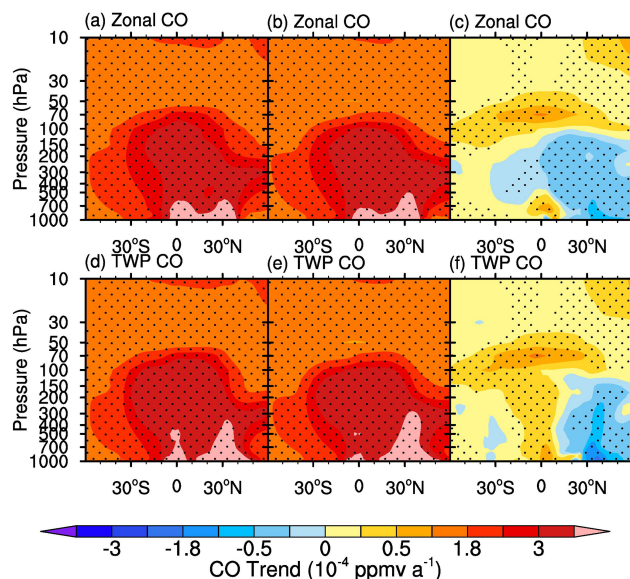


Figure 10. Latitude pressure cross sections of the trends of (a–c) the zonal mean CO concentration (10^{-4} ppmv a^{-1}) and (d–f) CO concentration (10^{-4} ppmv a^{-1}) over the TWP (100 – 180° E) in NDJFM during 1958–2017 in the Control simulation and Fixsst simulation, as well as their difference. Panels (a) and (d) are the CO trends in the Control simulation. Panels (b) and (e) are the results in the Fixsst simulation. Panels (c) and (f) are the results derived from the difference between the Control and Fixsst simulations. The trends over the dotted regions are statistically significant at the 95 % confidence level.

in CO by an extra 14 %. This indicates that the increased zonal mean CO in the TTL (Fig. 10c) is mainly transported through the western Pacific bands and highlights the importance of the upward motion over the TWP in elevating trace gases from the surface to the upper troposphere.

To understand the CO trends in the Control and Fixsst simulations and their differences, the trends of vertical velocity averaged over the globe and the TWP band are given in Fig. 11. The zonal mean w shows weak and even decreasing trends in the tropics, while the w over the TWP intensified in the Control simulation in NDJFM during 1958–2017. This is consistent with Fig. 5. While the SSTs fixed to climatological values, the zonal mean w shows weak trends and the w over the TWP shows significantly negative trends. The changes in the global SSTs therefore lead to the increase in the w over the TWP region, as indicated in the differences between the two simulations in Fig. 11f. In summary, the CO shows increasing trends (3.5 ppbv per decade) at 150 hPa over the TWP in NDJFM, during 1958–2017, induced by the changes in the surface emissions and the upward motion. The trends of CO at 150 hPa over the TWP in NDJFM during 1958–2017 in the Fixsst simulation mainly include the impact induced by the increased surface emissions, since the upward motion over the TWP in the Fixsst simulation shows weak trends. The difference between the Control and Fixsst simu-

lations indicates that the enhanced tropospheric upward motion over the TWP forced by the changes in the global SSTs leads to some extra increase in CO concentrations in the upper troposphere. It should be mentioned that the increasing trends in CO in the lower troposphere in Fig. 10f may be mainly caused by the changes in the horizontal winds. Girach and Nair (2014) suggested that enhanced deep convection and the subsequent intensified upward motion may lead to a decreased CO concentration in the lower troposphere and an increased CO concentration in the upper troposphere. The trends of horizontal winds at 925 hPa are shown in Fig. S8c. There are northerly trends over east Asia and northeasterly trends near the south of Asia (Fig. S8c), which suggests that more CO-rich air from east Asia and south Asia could be transported to the TWP in the Control simulation compared to the Fixsst simulation. Since the CO concentration in the lower troposphere over the northern Pacific is higher than that over southern Pacific, the northerly trends over the western and central Pacific may also contribute to the increased CO in the lower troposphere over the TWP in Fig. 10f.

As discussed in the introduction, the tropospheric trace gases enter the stratosphere mainly through the large-scale tropical upwelling associated with the BD circulation. The trends of the BDC in different model simulations and their differences are displayed in Fig. 12. The tropical upwelling of BDC (w^*) calculated using the TEM formula increased significantly in the lower stratosphere over the past few decades, as seen in the JRA55 data and the Control simulation (Fig. 12a and b). We found that the 70 hPa upward mass flux in NDJFM in the tropics (15°S – 15°N) increased by $2.8 \pm 1.9\%$ per decade (significant at the 95 % confidence level) in the JRA55 data from 1958 to 2017 (Fig. 12a) and $4.6 \pm 4.3\%$ per decade (significant at the 95 % confidence level) in the MERRA-2 data from 1980 to 2017 (Fig. S7b). From the ERA5 data, the 70 hPa upward mass flux in NDJFM increased in the Northern Hemisphere (0 – 15°N) at a rate of $5.0 \pm 2.8\%$ per decade (significant at the 95 % confidence level) but decreased significantly in the Southern Hemisphere (0 – 15°S) during 1958–2017 (Fig. S7a). On average, the trend of the 70 hPa upward mass flux in NDJFM in the tropics (15°S – 15°N) is not significant in ERA5. In fact, many previous studies have investigated the trends of BDC. For example, Abalos et al. (2015) investigated the trends of BDC derived from JRA55, MERRA, and ERA-Interim data during 1979–2012 and suggested that the BDC in JRA55 and MERRA significantly strengthened throughout the layer at 100–10 hPa with a rate of 2%–5% per decade, while the BDC in ERA-Interim shows weakening trends. Diallo et al. (2021) compared the trends of the BDC in the ERA5 and ERA-Interim during 1979–2018 and pointed out that the BDC in the ERA-Interim shows weakening trend and the BDC in the ERA5 strengthened at a rate of 1.5% per decade, which is more consistent with other studies. In the present study, we only focus on the trend of the BDC in the wintertime (NDJFM) in the tropics (15°S – 15°N) during 1958–

2017, which may lead to some differences between our result and those in the previous studies. Overall, the trends of the tropical upwelling of BDC derived from JRA55, MERRA-2 data, and the Control simulation are similar to those in previous studies using both reanalysis datasets and model results (e.g. Butchart et al., 2010; Abalos et al., 2015; Fu et al., 2019; Rao et al., 2019; Diallo et al., 2021). However, the tropical upwelling of the BDC decreased in ERA5 data in the tropics (15°S – 15°N), which are different from the results in JRA55 and MERRA-2.

In the Fixsst simulation, the trend of w^* is much weaker and not significant in most areas. The changes in the global SSTs, therefore, play an important role in the intensification of the shallow branch of the BDC, as shown by the differences between the two simulations in Fig. 12d. In summary, the tropical upwelling of the BDC is likely strengthened as shown in JRA55 and MERRA-2 reanalyses, as well as model simulations, although there are some uncertainties since the ERA5 data show a negative trend. This may impact on the transport of the tropospheric trace gases from the TTL to a higher altitude. The increased concentration of CO in the UTLS in Figs. 9c and 10f may be due to a combined effect of the strengthened tropical upwelling of the BD circulation and the enhanced upward motion over the TWP. The enhancement of upward motion over the TWP, which transported more tropospheric trace gases to the upper troposphere, works together with the strengthened BD circulation under global warming and may lead to an increase in tropospheric trace gases over the TWP in the lower stratosphere.

4 Summary and discussion

The recent trends of the upward motion from the lower to the upper troposphere in boreal winter over the TWP is investigated for the first time, based on the JRA55, ERA5, and MERRA-2 datasets and four WACCM4 simulations (Table 2). The upward motion at 150 hPa over the TWP in NDJFM increased by $8 \pm 3.1\%$ per decade and $3.6 \pm 3.3\%$ per decade in NDJFM from 1958 to 2017 in JRA55 and ERA5 reanalysis datasets, respectively (Table 3). Despite the possible discontinuities between the radiosonde era (after 1958) and the satellite era (after 1979), the upward motion at 150 hPa over the TWP in NDJFM increased by $7.5 \pm 7.1\%$ per decade during 1980–2017 in MERRA-2 data. Such intensification of the upward motion over the TWP also exist in the middle and lower troposphere in NDJFM in JRA55, ERA5, and MERRA-2, which can be confirmed by the WACCM4 model simulations. Comparing the results between the Control and Fixsst simulations with WACCM4, it is found that the trend of the upward motion over the TWP is closely related to the changes in global SSTs, especially the SST warming over the eastern maritime continent and tropical western Pacific (see the results from experiments R1 and R2 in Fig. 7). Warmer SSTs over the eastern mar-

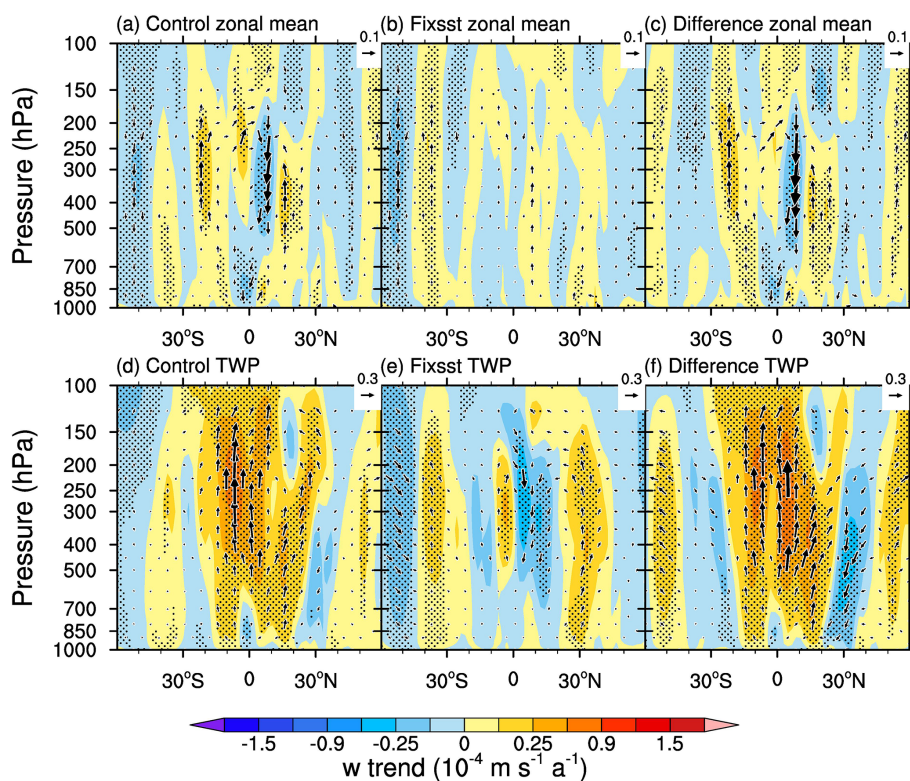


Figure 11. Same as Fig. 10 but for the trends of tropospheric w ($10^{-4} \text{ m s}^{-1} \text{ a}^{-1}$) and v ($10^{-1} \text{ m s}^{-1} \text{ a}^{-1}$). The shadings denote the trends of the w ($10^{-4} \text{ m s}^{-1} \text{ a}^{-1}$). The trends over the dotted regions are statistically significant at the 90 % confidence level.

itime continent and tropical western Pacific (approximately 0.5 K) lead to a strengthened Pacific Walker circulation, enhanced deep convection and approximately 27 % intensified upward motion at 150 hPa over the TWP as shown by the results from the experiments R1 and R2. The enhanced deep convection over the TWP could lead to a dryer lower stratosphere over the TWP, as the strong upward motion and the Rossby–Kelvin wave responses induce a colder tropopause over the TWP. It should be pointed out that the results in the present study are mainly based on the reanalyses data, and some uncertainties may exist. The availability of more high-resolution observations in the future may enhance the quality of the reanalysis data.

Results from the Control simulation indicate that the CO concentrations increased significantly from the surface to the stratosphere over the TWP. The CO at 150 hPa increased at a rate of approximately 3.4 ppbv per decade, with increased surface emissions and the enhanced upward motion over the TWP. Specifically, an enhancement of tropospheric upward motion and subsequent upward transport of trace gases over the TWP lead to an extra 6 % increasing trend in CO concentrations in the upper troposphere.

Furthermore, the upward mass fluxes at 70 hPa in the tropics ($15^\circ \text{ S}–15^\circ \text{ N}$) show strengthening trends at rates of $2.8 \pm 1.9 \%$ per decade and $4.6 \pm 4.3 \%$ per decade in JRA55 data (during 1958–2017) and MERRA-2 data (during 1980–

2017) in NDJFM, respectively, which is consistent with previous studies (e.g. Butchart et al., 2010; Fu et al., 2019; Rao et al., 2019). However, such an enhancement in the tropical upward mass flux at 70 hPa has large uncertainties since the ERA5 data show a negative and insignificant trend (Fig. S7a). The results from the Control and Fixsst simulations indicate that the elevated CO in the upper troposphere is further uplifted to the lower stratosphere by the intensified tropical upwelling of the BD circulation, which is mainly due to global SST warming, and leads to an increase in CO in the lower stratosphere. An extra 14 % increasing trend of CO at the layer of 150–70 hPa over the TWP is derived from the Control and Fixsst simulations.

Tropospheric trace gases and aerosols have important impacts on the stratospheric processes if they enter the stratosphere. For example, ozone-depleting substances, CH_4 and N_2O , could influence the stratospheric ozone significantly (e.g. Shindell et al., 2013; Wang et al., 2014), which also modifies the temperature in the stratosphere significantly through their strong radiative effects. Water vapour in the lower stratosphere, in particular, has a significant warming effect on the surface climate (Solomon et al., 2010). Therefore, changes in trace gases in the UTLS have important impacts on both tropospheric and stratospheric climate. Our results suggest that the upward motion over the TWP and the vertical component of the BDC at the lower stratosphere level

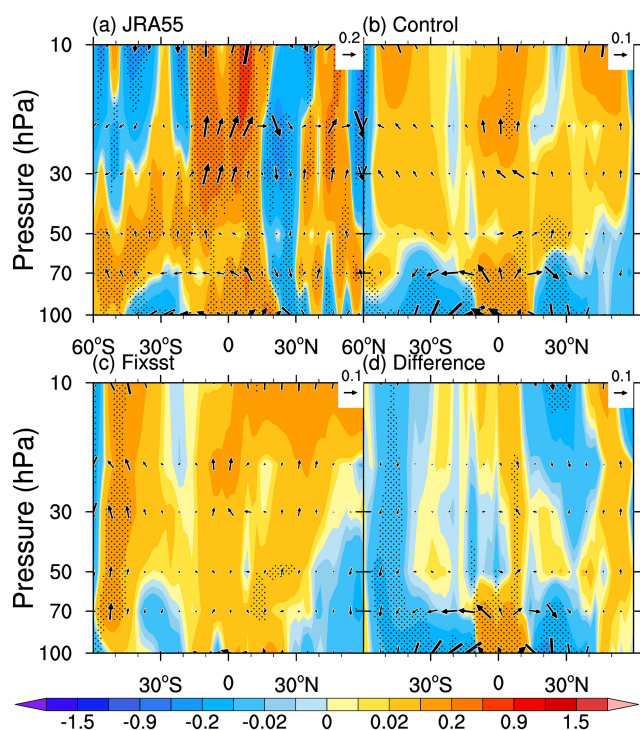


Figure 12. Trends of the BDC (vectors; the units in the horizontal and vertical components are 10^{-2} and 10^{-5} $\text{m s}^{-1} \text{a}^{-1}$, respectively) calculated using the TEM formula from (a) JRA55, (b) the Control simulation, (c) the Fixsst simulation, and (d) the difference between the Control simulation and the Fixsst simulation in NDJFM during 1958–2017. The shadings are the trends of the w^* (10^{-5} $\text{m s}^{-1} \text{a}^{-1}$). The trends of the vertical velocity over the dotted regions are statistically significant at the 90 % confidence level.

have been intensified. These results suggest that the emission from the maritime continent and surrounding areas may play a more important role in the stratospheric processes and the global climate. In addition, more very short-lived substances emitted from the tropical ocean could be elevated to the TTL by the enhanced convection and then transported into the stratosphere by the large-scale uplifts and exert important effects on the stratospheric chemistry. However, the quantitative impacts of the intensified upward motion over the TWP on tropospheric and stratospheric trace gases and aerosols and their climate feedbacks await further investigation with the use of more observations and model simulations.

Data availability. The authors gratefully acknowledge the data that were used in the present study as having been provided by the corresponding scientific groups. The JRA55 data are from <http://rda.ucar.edu/datasets/ds628.0/> (last access: 5 March 2022, Harada et al., 2016). The SST data are from HadISST <https://www.metoffice.gov.uk/hadobs/hadisst/data/download.html> (last access: 5 March 2022, Rayner et al., 2003). The ERA5 data and ERA5.1 data were extracted from <https://cds.climate.copernicus>.

[eu/#!/search?text=ERA5&type=dataset](https://search?text=ERA5&type=dataset) (last access: 5 March 2022, Hersbach et al., 2020). The MERRA-2 data are downloaded from <https://search.earthdata.nasa.gov/search?q=MERRA2&fst0=Atmosphere> (last access: 5 March 2022, Gelaro et al., 2017). The OLR data are from https://psl.noaa.gov/data/gridded/data.interp_OLR.html (last access: 5 March 2022, Liebmann and Smith, 1996).

Supplement. The supplement related to this article is available online at: <https://doi.org/10.5194/acp-22-4393-2022-supplement>.

Author contributions. KQ ran the models and wrote the first draft. WW provided suggestions about the statistical methods and model simulations. WT designed the study. RH, MX, and TW contributed to the writing. YP provided the data used in the study. All authors contributed to the improvement of the results.

Competing interests. The contact author has declared that neither they nor their co-authors have any competing interests.

Disclaimer. Publisher's note: Copernicus Publications remains neutral with regard to jurisdictional claims in published maps and institutional affiliations.

Acknowledgements. This research has been supported by the Supercomputing Center of Lanzhou University.

Financial support. This research has been supported by the Chinese Academy of Sciences (grant no. XDA17010106) and the National Natural Science Foundation of China (grant no. 42075055).

Review statement. This paper was edited by Peter Haynes and reviewed by two anonymous referees.

References

- Abalos, M., Legras, B., Ploeger, F., and Randel, W. J.: Evaluating the advective Brewer-Dobson circulation in three reanalyses for the period 1979–2012, *J. Geophys. Res.*, 120, 7534–7554, <https://doi.org/10.1002/2015JD023182>, 2015.
- Andrews, D. G. and McIntyre, M. E.: Planetary waves in horizontal and vertical shear: the generalized Eliassen-Palm relation and the mean zonal acceleration, *J. Atmos. Sci.*, 33, 2031–2048, 1976.
- Ashfold, M. J., Pyle, J. A., Robinson, A. D., Meneguz, E., Nadzir, M. S. M., Phang, S. M., Samah, A. A., Ong, S., Ung, H. E., Peng, L. K., Yong, S. E., and Harris, N. R. P.: Rapid transport of East Asian pollution to the deep tropics, *Atmos. Chem. Phys.*, 15, 3565–3573, <https://doi.org/10.5194/acp-15-3565-2015>, 2015.
- Bergman, J. W., Jensen, E. J., Pfister, L., and Yang, Q.: Seasonal differences of vertical-transport efficiency in the tropical tropopause layer: On the interplay between tropical deep convection, large-

- scale vertical ascent, and horizontal circulations, *J. Geophys. Res.*, 117, D05302, <https://doi.org/10.1029/2011JD016992>, 2012.
- Brewer, A. M.: Evidence for a world circulation provides by the measurements of helium and water vapor distribution in the stratosphere, *Q. J. Roy. Meteor. Soc.*, 75, 351–363, 1949.
- Butchart, N., Cionni, I., Eyring, V., Shepherd, T. G., Waugh, D. W., Akiyoshi, H., Austin, J., Brühl, C., Chipperfield, M. P., Cordero, E., Dameris, M., Deckert, R., Dhomse, S., Frith, S. M., Garcia, R. R., Gettelman, A., Giorgetta, M. A., Kinnison, D. E., Li, F., Mancini, E., McLandress, C., Pawson, S., Pitari, G., Plummer, D. A., Rozanov, E., Sassi, F., Scinocca, J. F., Shibata, K., Steil, B., and Tian, W.: Chemistry–Climate Model simulations of twenty-first century stratospheric climate and circulation changes, *J. Climate*, 23, 5349–5374, <https://doi.org/10.1175/2010JCLI3404.1>, 2010.
- Cane, M. A., Clement, A. C., Kaplan, A., Kushnir, Y., Pozdnyakov, D., Seager, R., Zebiak, S. E., and Murtugudde, R.: Twentieth-century sea surface temperature trends, *Science*, 275, 957–960, <https://doi.org/10.1126/science.275.5302.957>, 1997.
- Deeter, M. N., Edwards, D. P., Francis, G. L., Gille, J. C., Mao, D., Martínez-Alonso, S., Worden, H. M., Ziskin, D., and Andreae, M. O.: Radiance-based retrieval bias mitigation for the MOPITT instrument: the version 8 product, *Atmos. Meas. Tech.*, 12, 4561–4580, <https://doi.org/10.5194/amt-12-4561-2019>, 2019.
- Deser, C., Phillips, A. S., and Alexander, M. A.: Twentieth century tropical sea surface temperature trends revisited, *Geophys. Res. Lett.*, 37, L10701, <https://doi.org/10.1029/2010GL043321>, 2010.
- Diallo, M., Ern, M., and Ploeger, F.: The advective Brewer–Dobson circulation in the ERA5 reanalysis: climatology, variability, and trends, *Atmos. Chem. Phys.*, 21, 7515–7544, <https://doi.org/10.5194/acp-21-7515-2021>, 2021.
- Dobson G. M. B.: Origin and distribution of the polyatomic molecules in the atmosphere, *Proc. R. Soc. Lond. Ser. A.*, 236, 187–193, 1956.
- Duncan, B. N., Logan J. A., Bey, I., Megretskaia, I. A., Yantosca, R. M., Novelli, P. C., Jones, N. B., and Rinsland, C. P.: Global budget of CO, 1988–1997: Source estimates and validation with a global model, *J. Geophys. Res.*, 112, D22301, <https://doi.org/10.1029/2007JD008459>, 2007.
- Feng, W., Chipperfield, M. P., Dorf, M., Pfeilsticker, K., and Ricaud, P.: Mid-latitude ozone changes: studies with a 3-D CTM forced by ERA-40 analyses, *Atmos. Chem. Phys.*, 7, 2357–2369, <https://doi.org/10.5194/acp-7-2357-2007>, 2007.
- Fu, Q., Solomon, S., Pahlavan, H. A., and Lin, P.: Observed changes in Brewer–Dobson circulation for 1980–2018, *Environ. Res. Lett.*, 14, 114026, <https://doi.org/10.1088/1748-9326/ab4de7>, 2019.
- Fueglistaler, S., Wernli, H., and Peter, T.: Tropical troposphere-to-stratosphere transport inferred from trajectory calculations, *J. Geophys. Res.*, 109, D03108, <https://doi.org/10.1029/2003JD004069>, 2004.
- Fueglistaler, S., Desller, A. E., Dunkerton, T. J., Folkins, I., Fu, Q., and Mote P.: Tropical tropopause layer, *Rev. Geophys.*, 47, RG1004, <https://doi.org/10.1029/2008RG000267>, 2009.
- Fujiwara, M., Wright, J. S., Manney, G. L., Gray, L. J., Anstey, J., Birner, T., Davis, S., Gerber, E. P., Harvey, V. L., Hegglin, M. I., Homeyer, C. R., Knox, J. A., Krüger, K., Lambert, A., Long, C. S., Martineau, P., Molod, A., Monge-Sanz, B. M., San-tee, M. L., Tegtmeier, S., Chabrillat, S., Tan, D. G. H., Jackson, D. R., Polavarapu, S., Compo, G. P., Dragani, R., Ebisuzaki, W., Harada, Y., Kobayashi, C., McCarty, W., Onogi, K., Pawson, S., Simmons, A., Wargan, K., Whitaker, J. S., and Zou, C.-Z.: Introduction to the SPARC Reanalysis Intercomparison Project (S-RIP) and overview of the reanalysis systems, *Atmos. Chem. Phys.*, 17, 1417–1452, <https://doi.org/10.5194/acp-17-1417-2017>, 2017.
- Garfinkel, C. I., Waugh, D. W., Oman, L. D., Wang, L., and Hurwitz, M. M.: Temperature trends in the tropical upper troposphere and lower stratosphere: Connections with sea surface temperatures and implications for water vapor and ozone, *J. Geophys. Res.*, 118, 9658–9672, <https://doi.org/10.1002/jgrd.50772>, 2013.
- Garfinkel, C. I., Waugh, D. W., and Polvani, L. M.: Recent Hadley cell expansion: The role of internal atmospheric variability in reconciling modeled and observed trends, *Geophys. Res. Lett.*, 42, 10824–10831, <https://doi.org/10.1002/2015GL066942>, 2015.
- Garfinkel, C. I., Gordon, A., Oman, L. D., Li, F., Davis, S., and Pawson, S.: Nonlinear response of tropical lower-stratospheric temperature and water vapor to ENSO, *Atmos. Chem. Phys.*, 18, 4597–4615, <https://doi.org/10.5194/acp-18-4597-2018>, 2018.
- Gelaro, R., Mccarty, W., and Suárez, M. J.: The Modern-Era Retrospective Analysis for Research and Applications, Version 2 (MERRA-2), *J. Climate*, 30, 5419–5454, <https://doi.org/10.1175/JCLI-D-16-0758.1>, 2017 (data available at: <https://search.earthdata.nasa.gov/search?q=MERRA2&fst0=Atmosphere>, last access: 5 March 2022).
- Gettelman, A., Holton, J. R., and Douglass, A. R.: Simulations of water vapor in the lower stratosphere and upper troposphere, *J. Geophys. Res.*, 105, 9003–9023, <https://doi.org/10.1029/1999JD901133>, 2000.
- Gill, A. E.: Some simple solutions for heat-induced tropical circulation, *Q. J. Roy. Meteor. Soc.*, 106, 447–462, <https://doi.org/10.1002/qj.49710644905>, 1980.
- Girach, I. A. and Nair, P. R.: Carbon monoxide over Indian region as observed by MOPITT, *Atmos. Environ.*, 99, 599–609, <https://doi.org/10.1016/j.atmosenv.2014.10.019>, 2014.
- Haines, P. E. and Esler, J. G.: Determination of the source regions for surface to stratosphere transport: An Eulerian backtracking approach, *Geophys. Res. Lett.*, 41, 1343–1349, <https://doi.org/10.1002/2013GL058757>, 2014.
- Harada, Y., Kamahori, H., Kobayashi, C., Endo, H., Kobayashi, S., Ota, Y., Onoda, H., Onogi, K., Miyaoka, K., and Takahashi, K.: The JRA-55 Reanalysis: Representation of atmospheric circulation and climate variability, *J. Meteorol. Soc. Jpn.*, 94, 269–302, <https://doi.org/10.2151/jmsj.2016-015>, 2016 (data available at: <http://rda.ucar.edu/datasets/ds628.0/>, last access: 5 March 2022).
- Hersbach, H., Bell, B., Berrisford, P., Hirahara, S., Horányi, A., Muñoz-Sabater, J., Nicolas, J., Peubey, C., Radu, R., Schepers, D., Simmons, A., Soci, C., Abdalla, S., Abellan, X., Balsamo, G., Bechtold, P., Biavati, G., Bidlot, J., Bonavita, M., Chiara, G. D., Dahlgren, P., Dee, D., Diamantakis, M., Dragani, R., Flemming, J., Forbes, R., Fuentes, M., Geer, A., Haimberger, L., Healy, S., Hogan, R. J., Hólm, E., Janisková, M., Keeley, S., Laloyaux, P., Lopez, P., Lupu, C., Radnoti, G., Rosnay, P., Rozum, I., Vamborg, F., Villaume, S., and Thépaut, J.: The ERA5 global reanalysis, *Q. J. Roy. Meteor. Soc.*, 146, 1999–2049, <https://doi.org/10.1002/qj.3803>, 2020

- (data available at: <https://cds.climate.copernicus.eu/#!/search?text=ERA5&type=dataset>, last access: 5 March 2022).
- Highwood, E. J. and Hoskins, B. J.: The tropical tropopause, *Q. J. Roy. Meteor. Soc.*, 124, 1579–1604, <https://doi.org/10.1002/qj.49712454911>, 1998.
- Hitchcock, P.: On the value of reanalyses prior to 1979 for dynamical studies of stratosphere–troposphere coupling, *Atmos. Chem. Phys.*, 19, 2749–2764, <https://doi.org/10.5194/acp-19-2749-2019>, 2019.
- Holton, J. R., Haynes, P. H., McIntyre, M. E., Douglass, A. R., Rood, R. B., and Pfister, L.: Stratosphere–troposphere exchange, *Rev. Geophys.*, 33, 403–439, <https://doi.org/10.1029/95RG02097>, 1995.
- Hosking, J. S., Russo, M. R., Braesicke, P., and Pyle, J. A.: Tropical convective transport and the Walker circulation, *Atmos. Chem. Phys.*, 12, 9791–9797, <https://doi.org/10.5194/acp-12-9791-2012>, 2012.
- Hu, D., Tian, W., Guan, Z., Guo, Y., and Dhomse, S.: Longitudinal asymmetric trends of tropical cold-point tropopause temperature and their link to strengthened Walker circulation, *J. Climate*, 29, 7755–7771, <https://doi.org/10.1175/JCLI-D-15-0851.1>, 2016.
- Hu, D., Guan, Z., Tian, W., and Ren, R.: Recent strengthening of the stratospheric Arctic vortex response to warming in the central North Pacific, *Nat. Commun.*, 9, 1697, <https://doi.org/10.1038/s41467-018-04138-3>, 2018.
- Hu, P., Huangfu, J., Chen, W., and Huang, R.: Impacts of early/late South China Sea summer monsoon withdrawal on tropical cyclone genesis over the western North Pacific, *Clim. Dynam.*, 55, 1507–1520, <https://doi.org/10.1007/s00382-020-05339-7>, 2020.
- Huang, L., Jiang, J. H., Murray, L. T., Damon, M. R., Su, H., and Livesey, N. J.: Evaluation of UTLS carbon monoxide simulations in GMI and GEOS-Chem chemical transport models using Aura MLS observations, *Atmos. Chem. Phys.*, 16, 5641–5663, <https://doi.org/10.5194/acp-16-5641-2016>, 2016.
- Krüger, K., Tegtmeier, S., and Rex, M.: Long-term climatology of air mass transport through the Tropical Tropopause Layer (TTL) during NH winter, *Atmos. Chem. Phys.*, 8, 813–823, <https://doi.org/10.5194/acp-8-813-2008>, 2008.
- Levine, J. G., Braesicke, P., Harris, N. R. P., Savage, N. H., and Pyle, J. A.: Pathways and timescales for troposphere-to-stratosphere transport via the tropical tropopause layer and their relevance for very short lived substances, *J. Geophys. Res.*, 112, D04308, <https://doi.org/10.1029/2005JD006940>, 2007.
- Levine, J. G., Braesicke, P., Harris, N. R. P., and Pyle, J. A.: Seasonal and inter-annual variations in troposphere-to-stratosphere transport from the tropical tropopause layer, *Atmos. Chem. Phys.*, 8, 3689–3703, <https://doi.org/10.5194/acp-8-3689-2008>, 2008.
- L’Heureux, M. L., Lee, S., and Lyon, B.: Recent multi-decadal strengthening of the Walker circulation across the tropical Pacific, *Nat. Clim. Change*, 3, 571–576, <https://doi.org/10.1038/nclimate1840>, 2013.
- Liebmann, B. and Smith, C. A.: Description of a complete (interpolated) outgoing longwave radiation dataset, *B. Am. Meteorol. Soc.*, 77, 1275–1277, <http://www.jstor.org/stable/26233278> (last access: 5 March 2022), 1996 (data available at: https://psl.noaa.gov/data/gridded/data.interp_OLR.html, last access: 5 March 2022).
- Lin, P., Ming, Y., and Ramaswamy, V.: Tropical climate change control of the lower stratospheric circulation, *Geophys. Res. Lett.*, 42, 941–948, <https://doi.org/10.1002/2014GL062823>, 2015.
- Livesey, N. J., Logan, J. A., Santee, M. L., Waters, J. W., Doherty, R. M., Read, W. G., Froidevaux, L., and Jiang, J. H.: Interrelated variations of O₃, CO and deep convection in the tropical/subtropical upper troposphere observed by the Aura Microwave Limb Sounder (MLS) during 2004–2011, *Atmos. Chem. Phys.*, 13, 579–598, <https://doi.org/10.5194/acp-13-579-2013>, 2013.
- Livesey, N. J., Read, W. G., Wagner, P. A., Froidevaux, L., Lambert, A., Manney, G. L., Millán, L., Pumphrey, H. C., Santee, M. L., Schwartz, M. J., Wang, S., Fuller, R. A., Jarnot, R. F., Knosp, B. W., and Martinez, E.: EOS MLS Version 4.2x Level 2 data quality and description document, Tech. Rep., Jet Propulsion Laboratory, California Institute of Technology, Pasadena, CA, 1–162, <http://mls.jpl.nasa.gov/> (last access: 5 March 2022), 2015.
- Long, C. S., Fujiwara, M., Davis, S., Mitchell, D. M., and Wright, C. J.: Climatology and interannual variability of dynamic variables in multiple reanalyses evaluated by the SPARC Reanalysis Intercomparison Project (S-RIP), *Atmos. Chem. Phys.*, 17, 14593–14629, <https://doi.org/10.5194/acp-17-14593-2017>, 2017.
- Lu, J., Vecchi, G. A., and Reichler, T.: Expansion of the Hadley cell under global warming, *Geophys. Res. Lett.*, 34, L06805, <https://doi.org/10.1029/2006GL028443>, 2007.
- Lu, J., Xie, F., Sun, C., Luo, J., Cai, Q., Zhang, J., Li, J., and Tian, H.: Analysis of factors influencing tropical lower stratospheric water vapor during 1980–2017, *npj Clim. Atmos. Sci.*, 3, 35, <https://doi.org/10.1038/s41612-020-00138-7>, 2020.
- Ma, S., and Zhou, T.: Robust Strengthening and Westward Shift of the Tropical Pacific Walker Circulation during 1979–2012: A Comparison of 7 Sets of Reanalysis Data and 26 CMIP5 Models, *J. Climate*, 29, 3097–3118, <https://doi.org/10.1175/JCLI-D-15-0398.1>, 2016.
- Marsh, D. R., Mills, M. J., Kinnison, D. E., Lamarque, J., Calvo, N., and Polvani, L. M.: Climate change from 1850 to 2005 simulated in CESM1 (WACCM), *J. Climate*, 26, 7372–7391, <https://doi.org/10.1175/JCLI-D-12-00558.1>, 2013.
- McGregor, S., Timmermann, A., Stuecker, M. F., England, M. H., Merrifield, M., Jin, F., and Chikamoto, Y.: Recent Walker circulation strengthening and Pacific cooling amplified by Atlantic warming, *Nat. Clim. Change*, 4, 888–882, <https://doi.org/10.1038/nclimate2330>, 2014.
- Meng, Q., Latif, M., Park, W., Keenlyside, N. S., Semenov, V. A., and Martin, T.: Twentieth century Walker circulation change: Data analysis and model experiments, *Clim. Dynam.*, 38, 1757–1773, <https://doi.org/10.1007/s00382-011-1047-8>, 2012.
- Minganti, D., Chabrilat, S., Christophe, Y., Errera, Q., Abalos, M., Prignon, M., Kinnison, D. E., and Mahieu, E.: Climatological impact of the Brewer–Dobson circulation on the N₂O budget in WACCM, a chemical reanalysis and a CTM driven by four dynamical reanalyses, *Atmos. Chem. Phys.*, 20, 12609–12631, <https://doi.org/10.5194/acp-20-12609-2020>, 2020.
- Navarro, M. A., Atlas, E. L., Saiz-Lopez, A., Rodriguez-Lloveras, X., Kinnison, D. E., Lamarque, J., Tilmes, S., Filus, M., Harris, N. R. P., Meneguz, E., Ashfold, M. J., Manning, A. J., Cuevas, C. A., Schauffler, S. M., and Donets, V.: Airborne measurements of organic bromine compounds in the Pacific tropical tropopause layer, *P. Natl. Acad. Sci. USA*, 112, 13789–13793, <https://doi.org/10.1073/pnas.1511463112>, 2015.

- Newell, R. E., and Gould-Stewart, S.: A stratospheric fountain?, *J. Atmos. Sci.*, 38, 2789–2796, [https://doi.org/10.1175/1520-0469\(1981\)038<2789:ASF>2.0.CO;2](https://doi.org/10.1175/1520-0469(1981)038<2789:ASF>2.0.CO;2), 1981.
- Newton, R., Vaughan, G., Hints, E., Filus, M. T., Pan, L. L., Honomichl, S., Atlas, E., Andrews, S. J., and Carpenter, L. J.: Observations of ozone-poor air in the tropical tropopause layer, *Atmos. Chem. Phys.*, 18, 5157–5171, <https://doi.org/10.5194/acp-18-5157-2018>, 2018.
- Pan, L. L., Atlas, E. L., Salawitch, R. J., Honomichl, S. B., Bresch, J. F., Randel, W. J., Apel, E. C., Hornbrook, R. S., Weinheimer, A. J., Anderson, D. C., Andrews, S. J., Baidar, S., Beaton, S. P., Campos, T. L., Carpenter, L. J., Chen, D., Dix, B., Donets, V., Hall, S. R., Hanisco, T. F., Homeyer, C. R., Huey, L. G., Jensen, J. B., Kaser, L., Kinnison, D. E., Koenig, T. K., Lamarque, J.-F., Liu, C., Luo, J., Luo, Z. J., Montzka, D. D., Nicely, J. M., Pierce, R. B., Riemer, D. D., Robinson, T., Romashkin, P., Saiz-Lopez, A., Schaufli, S., Shieh, O., Stell, M. H., Ullmann, K., Vaughan, G., Volkamer, R., and Wolfe, G.: The Convective Transport of Active Species in the Tropics (CONTRAST) Experiment, *B. Am. Meteorol. Soc.*, 98, 106–128, <https://doi.org/10.1175/BAMS-D-14-00272.1>, 2016.
- Pan, L. L., Honomichl, S. B., Thornberry, T., Rollins, A., Bui, T. P., Pfister, L., and Jensen, E. E.: Observational Evidence of Horizontal Transport-Driven Dehydration in the TTL, *Geophys. Res. Lett.*, 46, 7848–7856, <https://doi.org/10.1029/2019GL083647>, 2019.
- Park, M., Randel, W. J., Emmons, L. K., and Livesey, N. J.: Transport pathways of carbon monoxide in the Asian summer monsoon diagnosed from Model of Ozon and Related Tracers (MOZART), *J. Geophys. Res.*, 144, D08303, <https://doi.org/10.1029/2008JD010621>, 2009.
- Qie, K., Qie, X., and Tian, W.: Increasing trend of lightning activity in the South Asia region, *Sci. Bull.*, 66, 78–84, <https://doi.org/10.1016/j.scib.2020.08.033>, 2021.
- Randel, W. J. and Jensen, E. J.: Physical processes in the tropical tropopause layer and their roles in a changing climate, *Nat. Geosci.*, 6, 169–176, <https://doi.org/10.1038/ngeo1733>, 2013.
- Randel, W. J., Park, M., Emmons, L., Kinnison, D., Bernath, P., Walker, K. A., Boone, C., and Pumphrey, H.: Asian monsoon transport of pollution to the Stratosphere, *Science*, 328, 611–613, <https://doi.org/10.1126/science.1182274>, 2010.
- Rao, J., Yu, Y., Guo, D., Shi, C., Chen, D., and Hu, D.: Evaluating the Brewer-Dobson circulation and its responses to ENSO, QBO, and the solar cycle in different reanalyses, *Earth Planet. Phys.*, 3, 166–181, <https://doi.org/10.26464/epp2019012>, 2019.
- Rayner, N., Parker, D., Horton, E., Folland, C. K., Alexander, L., Rowell, D. P., Kent, E. C., and Kaplan, A.: Global analyses of sea surface temperature, sea ice, and night marine air temperature since the late nineteenth century, *J. Geophys. Res.*, 108, 4407, <https://doi.org/10.1029/2002JD002670>, 2003 (data available at: <https://www.metoffice.gov.uk/hadobs/hadisst/data/download.html>, last access: 5 March 2022).
- Rosenlof, K. H.: How water enters the stratosphere, *Science*, 302, 1691–1692, <https://doi.org/10.1126/science.1092703>, 2003.
- Ryu, J. and Lee, S.: Effect of tropical waves on the tropical tropopause transition layer upwelling, *J. Atmos. Sci.*, 67, 3130–3148, <https://doi.org/10.1175/2010JAS3434.1>, 2010.
- Schoeberl, M. R., Jensen, E. J., Pfister, L., Ueyama, R., Avery, M., and Dessler, A. E.: Convective hydration of the upper troposphere and lower stratosphere, *J. Geophys. Res.*, 123, 4583–4593, <https://doi.org/10.1029/2018JD028286>, 2018.
- Sherwood, S. C.: A stratospheric “drain” over the maritime continent, *Geophys. Res. Lett.*, 27, 677–680, <https://doi.org/10.1029/1999GL010868>, 2000.
- Shindell, D. T., Pechony, O., Voulgarakis, A., Faluvegi, G., Nazarenko, L., Lamarque, J.-F., Bowman, K., Milly, G., Kovari, B., Ruedy, R., and Schmidt, G. A.: Interactive ozone and methane chemistry in GISS-E2 historical and future climate simulations, *Atmos. Chem. Phys.*, 13, 2653–2689, <https://doi.org/10.5194/acp-13-2653-2013>, 2013.
- Shirley, D., Stanley, W., and Daniel, C.: *Statistics for Research*, third edn., John Wiley & Sons Inc., Hoboken, New Jersey, p. 627, ISBN 0-471-26735-X, 2004.
- Simmons, A. J., Poli, P., Dee, D. P., Berrisford, P., Hersbach, H., Kobayashi, S., and Peubey, C.: Estimating low-frequency variability and trends in atmospheric temperature using ERA-Interim, *Q. J. Roy. Meteor. Soc.*, 140, 329–353, <https://doi.org/10.1002/qj.2317>, 2014.
- Sinnhuber, B.-M., Sheode, N., Sinnhuber, M., Chipperfield, M. P., and Feng, W.: The contribution of anthropogenic bromine emissions to past stratospheric ozone trends: a modelling study, *Atmos. Chem. Phys.*, 9, 2863–2871, <https://doi.org/10.5194/acp-9-2863-2009>, 2009.
- Solomon, S., Rosenlof, K. H., Portmann, R. W., Daniel, J. S., Davis, S. M., Sanford, T. J., and Plattner, G.-K.: Contributions of stratospheric water vapor to decadal changes in the rate of global warming, *Science*, 327, 1219–1223, <https://doi.org/10.1126/science.1182488>, 2010.
- Tegtmeier, S., Anstey, J., Davis, S., Dragani, R., Harada, Y., Ivanciu, I., Pilch Kedzierski, R., Krüger, K., Legras, B., Long, C., Wang, J. S., Wargan, K., and Wright, J. S.: Temperature and tropopause characteristics from reanalyses data in the tropical tropopause layer, *Atmos. Chem. Phys.*, 20, 753–770, <https://doi.org/10.5194/acp-20-753-2020>, 2020.
- Tokina, H., Xie, S. P., Deser, C., Kosaka, Y., and Okumura, Y. M.: Slowdown of the Walker circulation driven by tropical Indo-Pacific warming, *Nature*, 491, 439–443, <https://doi.org/10.1038/nature11576>, 2012.
- Uma, K. N., Das, S. S., Ratnam, M. V., and Suneeth, K. V.: Assessment of vertical air motion among reanalyses and qualitative comparison with very-high-frequency radar measurements over two tropical stations, *Atmos. Chem. Phys.*, 21, 2083–2103, <https://doi.org/10.5194/acp-21-2083-2021>, 2021.
- Wales, P. A., Salawitch, R. J., Nicely, J. M., Anderson, D. C., Canty, T. P., Baidar, S., Dix, B., Koenig, T. K., Volkamer, R., Chen, D., Huey, L. G., Tanner, D. J., Cuevas, C. A., Fernandez, R. P., Kinnison, D. E., Lamarque, J.-F., Saiz-Lopez, A., Atlas, E. L., Hall, S. R., Navarro, M. A., Pan, L. L., Schaufli, S. M., Stell, M., Tilmes, S., Ullmann, K., Weinheimer, A. J., Akiyoshi, H., Chipperfield, M. P., Deushi, M., Dhomse, S. S., Feng, W., Graf, P., Hossaini, R., Jöckel, P., Mancini, E., Michou, M., Morgenstern, O., Oman, L. D., Pitari, G., Plummer, D. A., Revell, L. E., Rozanov, E., Saint-Martin, D., Schofield, R., Stenke, A., Stone, K. A., Visionsi, D., Yamashita, Y., and Zeng, G.: Stratospheric injection of Brominated very short-lived substances: Aircraft observations in the western Pacific and representation in global models, *J. Geophys. Res.*, 123, 5690–5719, <https://doi.org/10.1029/2017JD027978>, 2017.

- Wang, W., Tian, W., Dhomse, S., Xie, F., Shu, J., and Austin, J.: Stratospheric ozone depletion from future nitrous oxide increases, *Atmos. Chem. Phys.*, 14, 12967–12982, <https://doi.org/10.5194/acp-14-12967-2014>, 2014.
- Wang, W., Matthes, K., and Schmidt, T.: Quantifying contributions to the recent temperature variability in the tropical tropopause layer, *Atmos. Chem. Phys.*, 15, 5815–5826, <https://doi.org/10.5194/acp-15-5815-2015>, 2015.
- Wang, W., Matthes, K., Omarani, N.-E., and Latif, M.: Decadal variability of tropical tropopause temperature and its relationship to the Pacific Decadal Oscillation, *Sci. Rep.*, 6, 29537, <https://doi.org/10.1038/srep29537>, 2016.
- Webster, P. J. and Lukas, R.: TOGA COARE: the coupled ocean-atmosphere response experiment, *B. Am. Meteorol. Soc.*, 73, 1377–1416, [https://doi.org/10.1175/1520-0477\(1992\)073<1377:TCTCOR>2.0.CO;2](https://doi.org/10.1175/1520-0477(1992)073<1377:TCTCOR>2.0.CO;2), 1992.
- Webster, P. J., Clayson, C. A., and Curry, J. A.: Clouds, radiation, and the diurnal cycle of sea surface temperature in the tropical western Pacific, *J. Climate*, 8, 1712–1730, [https://doi.org/10.1175/1520-0442\(1996\)009<1712:CRATDC>2.0.CO;2](https://doi.org/10.1175/1520-0442(1996)009<1712:CRATDC>2.0.CO;2), 1996.
- Xiao, Y., Jacob, D. J., and Turquety, S.: Atmospheric acetylene and its relationship with CO as an indicator of air mass age, *J. Geophys. Res.*, 112, D12305, <https://doi.org/10.1029/2006JD008268>, 2007.
- Xie, F., Li, J., Tian, W., Feng, J., and Huo, Y.: Signals of El Niño Modoki in the tropical tropopause layer and stratosphere, *Atmos. Chem. Phys.*, 12, 5259–5273, <https://doi.org/10.5194/acp-12-5259-2012>, 2012.
- Xie, F., Li, J., Tian, W., Li, Y., and Feng, J.: Indo-Pacific Warm Pool Area Expansion, Modoki Activity, and Tropical Cold-Point Tropopause Temperature Variations, *Sci. Rep.*, 4, 4552, <https://doi.org/10.1038/srep04552>, 2014a.
- Xie, F., Li, J., Tian, W., Zhang, J., and Shu, J.: The impacts of two types of El Niño on global ozone variations in the last three decades, *Adv. Atmos. Sci.*, 31, 1113–1126, <https://doi.org/10.1007/s00376-013-3166-0>, 2014b.
- Xie, F., Tian, W., Zhou, X., Zhang, J., Xia, Y., and Lu, J.: Increase in lower stratospheric water vapor in the past 100 years related to tropical Atlantic warming, *Geophys. Res. Lett.*, 47, e2020GL090539, <https://doi.org/10.1029/2020GL090539>, 2020.
- Zhou, X., Chen, Q., Li, Y., Zhao, Y., Lin, Y., and Jiang, Y.: Impacts of the Indo-Pacific warm pool on lower stratospheric water vapor: Seasonality and hemispheric contrasts, *J. Geophys. Res.*, 126, e2020JD034363, <https://doi.org/10.1029/2020JD034363>, 2021.